The Astrophysical Journal, 692:109–132, 2009 February 10 doi:10.1088/0004-637X/692/1/109

PROPAGATION OF SOLAR ENERGETIC PARTICLES IN THREE-DIMENSIONAL INTERPLANETARY MAGNETIC FIELDS

Ming Zhang[1,3], Gang Qin[2], and Hamid Rassoul[1]
[1] Department of Physics and Space Science, Florida Institute of Technology, Melbourne, Florida 32901, USA
[2] State Key Laboratory of Space Weather, Center for Space Science and Applied Research, Chinese Academy of Sciences, Beijing 100190, China
Received 2008 July 11; accepted 2008 October 15; published 2009 February 13

ABSTRACT

This paper presents a model calculation of solar energetic particle propagation in a three-dimensional interplanetary magnetic field. The model includes essentially all the particle transport mechanisms: streaming along magnetic field lines, convection with the solar wind, pitch-angle diffusion, focusing by the inhomogeneous interplanetary magnetic field, perpendicular diffusion, and pitch-angle dependent adiabatic cooling by the expanding solar wind. We solve the Fokker–Planck transport equation with simulation of backward stochastic processes in a fixed reference frame in which any spacecraft is roughly stationary. As an example we model the propagation of those high-energy ($E \gtrsim 10$ MeV) solar energetic particles in gradual events that are accelerated by large coronal mass ejection shocks in the corona and released near the Sun into interplanetary space of a Parker spiral magnetic field. Modeled with different scenarios, the source of solar energetic particles can have a full or various limited coverages of latitude and longitude on the solar surface. We compute the long-term time profiles of particle flux and anisotropy at various locations in the heliosphere up to 3 AU, from the ecliptic to high latitudes. Features from particle perpendicular diffusion are revealed. Our simulation reproduces the observed reservoir phenomenon of solar energetic particles with constraints on either solar particle source or the magnitude of perpendicular diffusion.

Key words: Sun: particle emission – Sun: coronal mass ejections (CMEs) – Sun: flares – Sun: magnetic fields – interplanetary medium

Online-only material: color figure

1. INTRODUCTION

The Sun occasionally emits energetic particles up to GeV energies. These particles are called solar energetic particles (SEPs). Because they are harmful to the health of astronauts working in space and electronic components on satellites, SEPs have become a focus of the NSF Space Weather programs and NASA Sun-Earth Connection programs. Although understanding of the subject has made significant progresses through several decades of studies with observations in space and theoretical modeling, many questions still remain. One of them is how SEPs propagate in a three-dimensional interplanetary magnetic field from their source on the Sun to Earth.

SEP events are divided into two general categories: impulsive SEP events and gradual SEP events. Impulsive events, with characteristics of low intensity, short duration, and enhanced He-3 and electrons relative to protons, are produced by solar flares. Gradual events are related to coronal mass ejections (CMEs) and they usually have high flux in protons and last longer, sometimes up to a month. The shock driven by the CME is responsible for the acceleration of ambient corona or interplanetary material to high energies. There are a large number of papers dealing with various aspects of SEP acceleration (see Lee 2005 and references therein).

Most of the SEPs are probably produced near the Sun. This is obviously true to impulsive events. For gradual event, the CME shock may continuously accelerate particle as it propagates out to interplanetary space. In many events, energetic particles, particularly those of high energies, are produced near the Sun, where the shock is fast, magnetic field is strong and seed particles are dense. From the source location near the Sun to 1 AU at the Earth's orbit, SEPs have to go through the interplanetary magnetic field with turbulence. A large body of works describe the SEP intensity observed near Earth by using the focused transport equation (Roelof 1969; Kallenrode 1993; Bieber et al. 1994; Droge 1994; Ruffolo 1995; Kallenrode & Wibberenz 1997; Ng & Reames 1994; Ng et al. 1999, 2003; Zank et al. 2000; Rice et al. 2003; Li et al. 2003; Lee 2005). Some of them self-consistently treat the wave excitation and particle acceleration based on the theory by Lee (1983), while a few of them include an evolving shock. Essentially, in all these studies, only the particle transport along interplanetary magnetic field lines is considered. The validity of these theories in application to observations is based on an assumption that the SEP events are spherically symmetric. Without such an assumption, all these calculations are subject to an arbitrary factor of normalization proportional to the total number of particles injected onto that field line. In other words, the calculation of the SEP intensity time profile for observations at any location can be arbitrarily altered by an assumption of longitudinal distribution of source particle injection strength.

It is obvious from straightforward theoretical arguments that any complete consideration of SEP events should include particle transport in realistic three-dimensional interplanetary magnetic fields. When a spacecraft at any location in the heliosphere observes a SEP event, the spacecraft does not sample the same field line because the solar wind carries the magnetic field at a radial speed of a few hundred km s^{-1}. If an event lasts a week, the spacecraft sees magnetic field lines emanating from a solar longitude range of $\sim 90^\circ$. Some SEP events can last over a month during which a spacecraft samples the entire range of solar longitude. Typical sizes of CME are only $\sim 45^\circ$–90° wide (Hundhausen 1993). The shock driven by

[3] Visiting State Key Laboratory of Space Weather, Center for Space Science and Applied Research, Chinese Academy of Sciences, Beijing 100190, China.

the CME may be larger than the CME, but is impossible for the shock to expand to all latitudes and longitudes in a very short time period of a few hours. If a CME is not centered near the west rim of the Sun as viewed from Earth, then we cannot guarantee direct magnetic connection to the CME shock at all times. The problem gets worse if we compare observations from spacecraft at very different heliographic latitudes because interplanetary magnetic field lines in the Parker model do not connect across latitudes. Furthermore, as the CME propagates outward from the Sun, magnetic connection to the particle source is time dependent; a spacecraft can be connected to different parts of the CME shock which presumably has different characteristics such as shock obliquity and shock speed. Even if the CME shock can expand over the entire solar surface, the shock strength is unlikely to be uniform, leading to a nonuniform source particle injection. Impulsive SEP events have shorter duration, but the SEP source must be localized on the field lines connected to the solar flare, as evident from observations of sharp drop-out of SEP flux in impulsive events (Mazur et al. 2000). Thus any nonuniformity of the SEP source strength inside the solar flare could invalidate the assumption of spherical symmetry.

One reason why perpendicular diffusion was ignored in previous studies of SEP transport in interplanetary space is that, according to the quasilinear theory for cosmic ray diffusion (Jokipii 1966), the perpendicular diffusion coefficient is usually much smaller than the parallel diffusion coefficient. However, observations show that perpendicular diffusion could be considerably large relative to parallel diffusion. For example, Dwyer et al. (1997) and Zhang et al. (2003) reported that the perpendicular to parallel diffusion coefficient ratio could approach or exceed unity for some particle events. It has been confirmed from test particle simulations that the perpendicular to parallel diffusion coefficient ratio could indeed be as large as unity with some prescribed magnetic turbulence (Giacalone & Jokipii 1999; Qin et al. 2002; Qin 2002). Theoretical studies also show that nonlinear effects could cause large perpendicular diffusion (Matthaeus et al. 2003; Shalchi et al. 2004; Qin 2007).

Observations by multiple spacecraft often show profiles of SEP events at very different locations in the inner heliosphere are somehow related. Using simultaneous observation of SEP events from Ulysses and another spacecraft at Earth's orbit, McKibben et al. (2003) and Lario et al. (2003) found that the particle fluxes measured at two locations of very different radial distances, latitudes, and longitudes often reach an equal level (within a small $\sim$ 2–3 factor) in the decay phase of large SEP events, no matter where is the event's source on the Sun. The SEP fluxes in initial phase, however, can be very different by several orders of magnitude, depending on where the spacecraft is relative to the solar source. These periods of small radial, latitude, and longitude gradient of particle intensity were first noted by McKibben (1972) and were later named "reservoirs" by Roelof et al. (1992). Those periods of equal intensity have been observed during isolated large SEP events as well as during episode of solar events. The formation of energetic particle reservoirs is observed not only in protons, but also in heavy ions and energetic electrons (Maclennan et al. 2001; Lario et al. 2003). After reaching a uniform reservoir the particle intensities everywhere decrease at an approximately the same rate in time, which can sometimes last for more than a month. In addition, Reames et al. (1997) reported that the particle intensities of very different energies decrease at the same decay rate. Currently there is no consensus on the mechanisms for the formation of SEP reservoirs. McKibben (1972) and McKibben et al. (2003) suggested an effective cross-field diffusion to distribute the particles uniformly, while Roelof et al. (1992) and Reames et al. (1997) involved some kind of a diffusion barrier produced by interplanetary CME or shocks to contain the particles long enough for them to distribute uniformly through normal diffusion and adiabatic cooling. However, none of these theories have gone through detailed model calculation to reproduce the observed properties.

In order to compare the SEP event observed on different field lines, a complete model calculation has to consider particle transport in three dimension including the effect of radial convection of the magnetic field with the solar wind. This is the purpose of this paper.

We start with an equation of a SEP propagation containing all the transport mechanisms: pitch-angle diffusion, magnetic focusing, streaming along magnetic field lines, convection, cross-field diffusion, and adiabatic cooling. The equation is solved numerically through simulation of stochastic processes. For simplicity, in this first presentation we concentrate on the propagation of high-energy SEPs from gradual events in a simple steady state Parker interplanetary magnetic field with no disturbances from shocks, ICMEs, or other solar wind structures. Applications of this code to more complicated interplanetary magnetic field configures and solar particle sources will be the subject of our future work. Time profiles of SEP fluxes and anisotropies at various locations are computed and compared. We find that reservoirs of SEPs can form without involving deliberate diffusion barriers from shocks or ICMEs. The role of cross-field diffusion will be discussed.

2. MODEL

The basic equation that governs the gyrophase-averaged distribution function $f(\mathbf{x}, \mu, p, t)$ of SEPs as a function of spatial location $\mathbf{x}$, particle momentum p, pitch-angle cosine μ and time t can be written as

$$\frac{\partial f}{\partial t} = \nabla \cdot \boldsymbol{\kappa}_\perp \cdot \nabla f - (v\mu\hat{\mathbf{b}} + \mathbf{V}_{sw}) \cdot \nabla f + \frac{\partial}{\partial \mu} D_{\mu\mu} \frac{\partial f}{\partial \mu} + \left[\frac{(1-\mu^2)v}{2L_B} - \frac{\mu(1-\mu^2)}{2} (\nabla \cdot \mathbf{V}_{sw} - 3\hat{\mathbf{b}}\hat{\mathbf{b}} : \nabla \mathbf{V}_{sw}) \right] \frac{\partial f}{\partial \mu} + \left[\frac{1-\mu^2}{2} (\nabla \cdot \mathbf{V}_{sw} - \hat{\mathbf{b}}\hat{\mathbf{b}} : \nabla \mathbf{V}_{sw}) + \mu^2 \hat{\mathbf{b}}\hat{\mathbf{b}} : \nabla \mathbf{V}_{sw} \right] p \frac{\partial f}{\partial p}, \quad (1)$$

where the terms on the right-hand side are cross-field spatial diffusion $\boldsymbol{\kappa}_\perp$ tensor, streaming along the ambient magnetic field direction $\hat{\mathbf{b}}$ with speed v and pitch-angle cosine μ, convection with the solar wind $\mathbf{V}_{sw}$, pitch-angle diffusion $D_{\mu\mu}$, magnetic focusing with focal length $L_B = (\hat{\mathbf{b}} \cdot \nabla \ln B)^{-1}$ in the nonuniform ambient interplanetary magnetic field B, pitch-angle change due to anisotropic adiabatic cooling by the solar wind, and momentum change through adiabatic cooling. The origin of the first-order terms can be found in several previous literatures (Roelof 1969; Skilling 1971; Ruffolo 1995; Isenberg 1997; Qin et al. 2004, 2006; Zhang 2006). The second-order terms represent the effects of magnetic turbulence. The equation is truncated up to the diffusion as approximated by quasilinear theory, even though the level of interplanetary magnetic field turbulence can sometimes be comparable to or higher than the ambient magnetic field strength. Normally, there should be 10 independent Fokker–Planck diffusion coefficients (e.g.,

Schlickeiser 2002; Zhang 2006). Because the propagation speed of magnetic field turbulence in the interplanetary medium, which is typically the Alfven speed or fast-mode MHD wave speed, is much less than the speed of particles, adiabatic cooling by the solar wind dominates particle momentum change by fluctuating the electric field in the turbulence, so all the diffusion terms related to p disappear. If we further assume that magnetic field turbulence is random, only pitch-angle diffusion $D_{\mu\mu}$ and cross-field diffusion $\boldsymbol{\kappa}_\perp$ are not zero (Jokipii 1966). We neglect particle gradient/curvature drift in the nonuniform magnetic field because the magnetic field in the inner heliosphere is too strong and energies of typical SEPs are not high enough. Equation (1) is the most complete transport equation under the above conditions.

Note that the transport equation is written with variables in mixed reference frames, with spatial coordinates in the fixed frame and particle momentum and pitch angle in the solar wind frame (see Chapter 12 in Schlickeiser 2002; Zhang 2006). Although it is easy to transform the equation into the solar wind frame or solar corotating frame for the spatial coordinates, we choose to use the fix reference frame for the spatial coordinates so that the calculation of SEP at any roughly stationary spacecraft is straightforward even though the Sun with the source particle location is rotating. In the fixed reference frame, both spiral magnetic field lines and particles are convecting with the solar wind speed, thus taking care of the apparent corotation of the interplanetary magnetic field. The momentum and pitch-angle variables are in the solar wind plasma frame, in which the average electric field is always zero and the distribution is roughly gyrotropic; otherwise, the transport equation will be different and much more complicated. When comparing the calculation result to any observation by a spacecraft, we have to perform a Galileo transform for the momentum and pitch angle. Compton–Getting effect arises from Galileo transformation (see, e.g., Zhang 2005). If the particle speed is much larger than the solar wind speed as seen by the spacecraft, the Galileo transform will result in little change in momentum and pitch angle with little Compton–Getting anisotropy. So essentially Galileo transform is not necessary for SEPs with energies above a few MeV/n.

Transport Equation (1) is also good for describing particle acceleration by CME shocks. Only at very low particle energies where the particle speed is not much greater than the shock speed, the diffusive transport behavior breaks down. This has been a formidable problem of particle injection for diffusive shock acceleration theory. Currently there is no clear way to estimate particle injection from low-energy or thermal particles. The rate of particle injection is a crucial parameter for the calculation of the particle flux produced by shock acceleration. So without a theory for particle injection, comparison of absolute particle fluxes at various locations connected to different parts of the CME shock is essentially meaningless even when one has a perfect theory for diffusive shock acceleration that may include self-consistent wave–particle interactions. Therefore, in this paper we avoid the problems of particle injection and acceleration by directly inputting a source of accelerated particles as a product of either the CME shock or solar flare.

SEPs can be continuously injected onto the field lines connected out into interplanetary space. The injection can occur quite far out from the Sun as some CME shocks can propagate to very large radial distances with enough strength. However, we expect that this will mainly happen to low-energy particles because as the shock slows down, the magnetic field becomes weaker and low-energy seed particles get more tenuous as the shock propagates outward. The above transport equation still can handle continuous particle injections with time dependent source locations and injection rate. However, in this paper, for the purpose of simplicity, we concentrate on high-energy SEPs that are accelerated and released into the system near the Sun. The particle injection is then like a point source in the radial dimension, which is particularly a valid assumption for observations far out at 1 AU or larger radial distances.

We choose to use boundary condition of Equation (1) at the interface with solar corona as the injected source of SEPs. The boundary value is a function of time t, particle momentum p, as well as solar longitude ϕ and colatitude θ if an event has a limited coverage on the Sun. We assume this boundary condition as

$$f_b(\mathbf{x}, \mu, p, t)\,|_{r=R_s} = p^{-\gamma}\frac{1}{t}\exp\left(-\frac{T_c}{t}-\frac{t}{T_l}\right)a(\phi,\theta), \quad (2)$$

where R_s is the radial distance at which SEPs are released into the system, γ the spectral index of source particles, T_c and T_l time constants controlling the time profile of particle release from the solar corona, and $a(\phi, \theta)$ a function specifying the longitudinal and latitudinal dependence of SEP source strength. The power-law form of a source particle spectrum is intended to be consistent with diffusive shock acceleration. The boundary condition is isotropic in terms of the particle pitch angle because of the expected high magnetic turbulence near the shock in the corona. The time profile used in Equation (2) is taken from Reid (1964). Although this form is originally based on an assumption of lateral diffusion in the corona, we choose to use it as a pulse of particle injection when the shock is near the Sun. Typical values of T_c and T_l are a few hours, much shorter than the time scale to reach the maximum SEP flux or the decay phase of SEP events. The time profile of source particle injection is very much likely from a short pulse. At late time of an SEP event, all the injection profiles behave like a $\delta(t)$ injection. There is also a boundary condition at the outer boundary. We choose it to be an absorptive boundary at a radial distance $R_o >$ 10 AU, far out enough that it will not affect the calculation result in the inner heliosphere unless an abnormally large mean free path is used. Alternatively, one may choose to add a source term in the transport Equation (1) instead of a boundary value condition as particle injection. If the particles are all injected at the inner boundary, the nonhomogeneous differential equation with a source term can be easily transformed into the above boundary value problem. In fact, several previous models with focused transport equation also used boundary values to specify particle injection on the Sun (Kallenrode & Wibberenz 1997).

Transport Equation (1) is a five-dimensional parabolic partial differential equation with a Dirichlet boundary condition. We use a method of simulating stochastic processes to solve the equation numerically. Both the finite difference and finite element methods will run into difficulty with computation power if one wants to have a decent resolution in all the five dimensions. In our method, the Fokker–Planck diffusion Equation (1) is recast into five time-backward stochastic differential equations for spatial location, pitch-angle cosine, and momentum of individual psudeoparticles that represent the value of the particle distribution function (see Zhang 1999),

$$d\mathbf{x}(s) = \sqrt{2\boldsymbol{\kappa}_\perp}\cdot d\mathbf{w}(s) + (\nabla\cdot\boldsymbol{\kappa}_\perp - v\mu(s)\hat{\mathbf{b}} - \mathbf{V}_{sw})ds \quad (3)$$

$$d\mu(s) = \sqrt{2\max(D_{\mu\mu}, 0)}dw(s) + \left[\frac{\partial D_{\mu\mu}}{\partial \mu} + \frac{(1-\mu^2(s))v}{2L_B} - \frac{\mu(s)(1-\mu^2(s))}{2}(\nabla\cdot\mathbf{V}_{sw} - 3\hat{\mathbf{b}}\hat{\mathbf{b}}:\nabla\mathbf{V}_{sw})\right]ds \tag{4}$$

$$dp(s) = \left[\frac{1-\mu^2(s)}{2}(\nabla\cdot\mathbf{V}_{sw} - \hat{\mathbf{b}}\hat{\mathbf{b}}:\nabla\mathbf{V}_{sw}) + \mu^2(\hat{\mathbf{b}}\hat{\mathbf{b}}:\nabla\mathbf{V}_{sw})\right]p(s)ds, \tag{5}$$

where $dw(s)$ is a Wiener process as a function of s which is the time running backward. $dw(s)$ can be generated by random numbers with a Gaussian distribution with a standard deviation of $\sqrt{ds}$. There are three independent dw's in Equations (3)–(5). The function max in Equation (4) takes the maximum value of all its arguments. Because $D_{\mu\mu} \propto (1-\mu^2)$ becomes negative for $\mu^2 > 1$, the maximum value of either 0 or $D_{\mu\mu}$ makes sure the numerical simulation returns to the valid domain of $[-1, 1]$, even if it makes occasional excursion outside its domain. In this way we fulfill the boundary condition at $\mu = \pm 1$, which in theory should be impassible nodes. The simulation of stochastic processes starts at the location $\mathbf{x}$, pitch-angle μ, momentum p, and time t where the solution to the particle distribution function is sought, i.e., $\mathbf{x}(0) = \mathbf{x}$, $\mu(0) = \mu$, and $p(0) = p$ at initial backward time $s = 0$ at time t.

The stochastic differential equation is like a first-order ordinary differential equation. We solve the stochastic differential Equations (3)–(5) with an Euler scheme (Kloeden & Platen 1992). Because particle streaming along the magnetic field line is much faster than other transport terms, we use a fourth-order Range–Kutta scheme (Press et al. 1991) for the integration of that part. Like ordinary differential equation, the method does not suffer numerical instability even with very tiny time steps. Numerical errors seem to be diminished when stochastic terms are introduced because the randomness tends to cancel numerical error propagating over the calculation. All simulations exit when the stochastic trajectories hit the boundaries for the first time at $\mathbf{x}_e$, μ_e, p_e and $s = \tau_e$ or time $t_e = t - \tau_e$. Then the exact solution to Equation (1) is the expectation value of the boundary values at the exit points

$$f(\mathbf{x}, \mu, p, t) = \langle f_b(\mathbf{x}_e, \mu_e, p_e, t_e)\rangle = \frac{\sum_{i=1}^{N} f_b(\mathbf{x}_e^i, \mu_e^i, p_e^i, t_e^i)}{N}, \tag{6}$$

where $\langle\,\rangle$ denotes the expectation or the average value of whatever inside it and N is the total number of trial trajectories. Its uncertainty can be estimated through error propagation

$$\delta f = \frac{\sqrt{\sum_{i=1}^{N} f_b^2(\mathbf{x}_e^i, \mu_e^i, p_e^i, t_e^i)}}{N}, \tag{7}$$

where we assume that each trajectory carries a 100% uncertainty. Typically, if the distribution of boundary values does not vary considerably, we just need to simulate a few thousands stochastic trajectories to achieve a relative error bar $\delta f/f$ of less than 3%, which is good enough for many applications. However, since the injection of SEPs is usually strongly peaked within a few hours after the onset of source injection, only those exit points reaching the source in a correct time window can make significant contribution to the expectation value in Equation (6). Efficiency of simulation becomes intolerably low if we just compute the solution for one time point. However, the efficiency can be improved if we want to compute an entire time profile of the particle flux. The improvement is made by recording the total transport time from the observer to the inner source τ_e. Those stochastic trajectories with a $t - \tau_e$ that falls within a few hours of injection window will make a significant contribution. Eventually, all of simulated stochastic trajectories will be used if the transport time τ_e is not too long.

The interplanetary magnetic field and solar wind which the particles travel through are taken from the steady state Parker model (Parker 1963). Rates of particle transport processes such as adiabatic cooling and focal length can be computed from the field and plasma model using vector calculus. The steady state interplanetary medium ensures that the above method to improve simulation efficiency can be used.

There is another factor that can lower the simulation efficiency. For many common choices of transport coefficients, most time-backward stochastic trajectories take very long time to get back to the particle source at the inner boundary. This happens because the time-backward focusing effect tends to reflect the trajectory back to the interplanetary space (mirroring effect). Qin et al. (2005) modified the transport equation by solving $u(\mathbf{x}, \mu, p, t) = f(\mathbf{x}, \mu, p, t)/f_0(\mu)$, where $f_0(\mu)$ is a prescribed function of μ, instead of solving f directly. The equation for u is still in a form belonging to a more general parabolic differential equation with an additional decay term equal to $c(\mathbf{x}, \mu, p, t)u(\mathbf{x}, \mu, p, t)$ (Zhang 1999), where

$$c(\mathbf{x}, \mu, p, t) = \frac{\partial}{f_0(\mu)\partial\mu}D_{\mu\mu}\frac{\partial f_0(\mu)}{\partial\mu} + \left[\frac{(1-\mu^2)v}{2L_B} - \frac{\mu(1-\mu^2)}{2} \times (\nabla\cdot\mathbf{V}_{sw} - 3\hat{\mathbf{b}}\hat{\mathbf{b}}:\nabla\mathbf{V}_{sw})\right]\frac{\partial f_0(\mu)}{f_0(\mu)\partial\mu}. \tag{8}$$

The equation for $u(\mathbf{x}, \mu, p, t)$ can be solved in a similar way as f using the above described stochastic simulation, except the boundary value is modified and stochastic trajectories are governed by a different stochastic differential equation (see Zhang 1999). Substituting back the relationship between $u(\mathbf{x}, \mu, p, t)$ and $f(\mathbf{x}, \mu, p, t)$, we can get a solution for $f(\mathbf{x}, \mu, p, t)$ by this modified formula

$$f(\mathbf{x}, \mu, p, t) = f_0(\mu)\left\langle\frac{f_b(\mathbf{x}_e, \mu_e, p_e, t_e)}{f_0(\mu_e)} \times \exp\left(\int_0^{\tau_e} c(\mathbf{x}(s), \mu(s), p(s), t-s)ds\right)\right\rangle \tag{9}$$

with a modified stochastic differential equation for $\mu(s)$

$$d\mu(s) = \sqrt{2\mathrm{Max}(D_{\mu\mu}, 0)}dw(s) + \left[2D_{\mu\mu}\frac{\partial f_0(\mu)}{f_0(\mu)\partial\mu} + \frac{\partial D_{\mu\mu}}{\partial\mu} + \frac{(1-\mu^2(s))v}{2L_B} - \frac{\mu(s)(1-\mu^2(s))}{2} \times (\nabla\cdot\mathbf{V}_{sw} - 3\hat{\mathbf{b}}\hat{\mathbf{b}}:\nabla\mathbf{V}_{sw})\right]ds, \tag{10}$$

where the equation contains an additional drift term $2D_{\mu\mu}\frac{\partial f_0(\mu)}{f_0(\mu)\partial\mu}$ to drive $\mu(s)$ to a desirable direction.

Table 1
Model Parameters Used in the Calculations

Parameter	Formula	Values
Inner boundary	$r = R_s$	$R_s = 0.05$ AU
Outer boundary	$r = R_o$	$R_o = 50$ AU
Solar rotation	$\Omega = 2\pi/T$	$T = 27.27$ day
Solar wind	$\mathbf{V}_{sw} = V_{sw}\hat{\mathbf{r}}$	$V_{sw} = 400$ km s^{-1}
Magnetic field	$\mathbf{B} = \frac{B_0}{r^2}(\hat{\mathbf{r}} - \frac{\Omega r \sin\theta}{V_{sw}}\hat{\phi})$	$B_0 = 3.54$ nT AU^2
Pitch-angle diffusion	$D_{\mu\mu} = D_0(1-\mu^2)vp^{-b_1}(h + \lvert\mu\rvert^{q-1})k(\mathbf{x})$	$D_0 = $ const
		$b_1 = 2/3$
		$h = 0.2$
		$q = 5/3$
		$k(\mathbf{x}) = (\cos\Psi)^{-2} = (B/B_r)^2$
Perpendicular diffusion	$\boldsymbol{\kappa}_\perp = \kappa_\perp(\mathbf{I} - \hat{\mathbf{b}}\hat{\mathbf{b}})$	$\kappa_0 = $ const
	with $\kappa_\perp = \kappa_0(v/c)(p/p_0)^{b_2}(B_\oplus/B)$	$b_2 = 2/3$
		$p_0 = 1$ GeV/c

Notes. We choose D_0 so that at 100 MeV $\lambda_r = \lambda_{||}\cos^2\Psi$ 0.2 AU for large mean free path and 0.05 AU for small mean free path. $\kappa_0 = 2 \times 10^{20}$ cm^2 s^{-1} is chosen for a low perpendicular transport condition and $\kappa_0 = 5 \times 10^{20}$ cm^2 s^{-1} for a high perpendicular transport. The perpendicular diffusion tensor can be made anisotropic by assigning different κ_0 values for different perpendicular directions.

The equations for $\mathbf{x}(s)$ and $p(s)$ remain the same as before. Qin et al. (2006) chose a form $f_0 = 1 + a_1\mu$ with $a_1 = const < 1.0$. The additional drift term in Equation (10) is positive, so $\mu(s)$ increases and it accelerates $\mathbf{x}(s)$ in the $-\hat{\mathbf{b}}$ direction. The amount of acceleration back towards the Sun can be controlled with the choice of a_1 value. If we want to look at the SEP flux in the early phase of an event, we put in a larger a_1 (typically 0.1–0.5), so that most stochastic trajectories exit with a short τ_e. Smaller a_1 values of 0.02–0.1 are suitable if we want to look at a long decay phase of a SEP event with a decent statistics. The design of $f_0(\mu)$ is to increase the simulation speed only, and it does not change the answer to $f(\mathbf{x}, \mu, p, t)$ so we will not list the a_1 values used in all of our following model runs.

Table 1 lists the model parameters we use for our simulation runs. The parameters for the solar wind and magnetic field represent a typical ambient interplanetary condition. The form of pitch-angle diffusion coefficient is chosen to match the result of quasi-linear theory with some nonlinear corrections (Beeck & Wibberenz 1986; Qin et al. 2005). The parallel mean free path is related to pitch-angle diffusion by

$$\lambda_{||} = \frac{3v}{8}\int_{-1}^{1}\frac{(1-\mu^2)^2}{D_{\mu\mu}}d\mu. \quad (11)$$

Parameter b_1 in Table 1 characterizes the momentum dependence of $\lambda_{||}$, while the function $k(\mathbf{x})$ specifies the spatial dependence. If we assume $k(\mathbf{x}) = (\cos\Psi)^{-2}$, where Ψ is the angle of the local magnetic field direction to the radial line, the parallel mean free path projected in the radial direction $\lambda_r = \lambda_{||}\cos^2\Psi$ is constant, a spatial dependence also used by other models (e.g., Kallenrode & Wibberenz 1997). An $h \neq 0$ is needed to make particles scatter across the zero pitch-angle cosine or make particles turn around. The parameter D_0 is a constant to determine the value of the radial mean free path. We typically use $\lambda_r = 0.2$ AU at 100 MeV energy for a condition of high mean free path and $\lambda_r = 0.05$ AU for a low mean free path situation. The form for the perpendicular diffusion tensor $\boldsymbol{\kappa}_\perp$ is borrowed from typical cosmic ray modulation simulation (Potgieter 1998). Note that the diffusion tensor could be a function of μ, while the diffusion tensor in cosmic ray transport equation is its average over all $\mu = [-1, 1]$. However, if we assume that the diffusion coefficient is independent of μ, then the two perpendicular diffusion coefficients are exactly the same. The assumption of μ-independence probably will not very much affect the calculation result here, because by the time when the effect of perpendicular diffusion is noticeable, the distribution has already become nearly isotropic through much faster pitch-angle scattering. We typically use a value of $b_2 = 2/3$ and $\kappa_0 = 2 \times 10^{20}$ cm^2 s^{-1} for low perpendicular diffusion and $\kappa_0 = 5 \times 10^{20}$ cm^2 s^{-1} for high perpendicular diffusion condition. A $\kappa_0 = 2 \times 10^{20}$ cm^2 s^{-1} corresponds to a perpendicular mean free path of 4/3000 AU for particles of $p = 1$ GeV/c or 433 MeV energy at Earth location ($\sim$ 1 AU Equator). Perpendicular diffusion gets smaller at radial distances closer to the Sun as it is inversely proportional to local magnetic field strength.

3. RESULTS

3.1. Validation

Figure 1 compares our result with a solution of focused transport equation using the finite difference method (Kallenrode & Wibberenz 1997). Because the code by Kallenrode available to us handles only SEP propagation along field lines without the effect of adiabatic cooling, we turn off adiabatic cooling and perpendicular diffusion in our run in order to make direct comparison. Both models specify the inner boundary condition as a source of particle injection. All model parameters are exactly the same. Because our time-backward simulation can only solve for the particle distribution function at one specific location in the phase space of position, momentum and pitch angle in one simulation, then the calculation of the omnidirectional particle flux would require obtaining solutions for all pitch angles. This would be too costly in computation power. Instead, we just calculate the solution of the particle distribution function at $\mu = -1, 0, 1$ at one location of space $\mathbf{x}$ and momentum p. The omnidirectional particle flux j_0 and flux anisotropies of first-order A_1 and second-order A_2 are calculated through harmonic expansion up to the second order

$$j_0 = 4\pi p^2\frac{f(\mu=-1) + 2f(\mu=0) + f(\mu=1)}{4} \quad (12)$$

$$A_1 = \frac{2[f(\mu=1) - f(\mu=-1)]}{f(\mu=-1) + 2f(\mu=0) + f(\mu=1)} \quad (13)$$

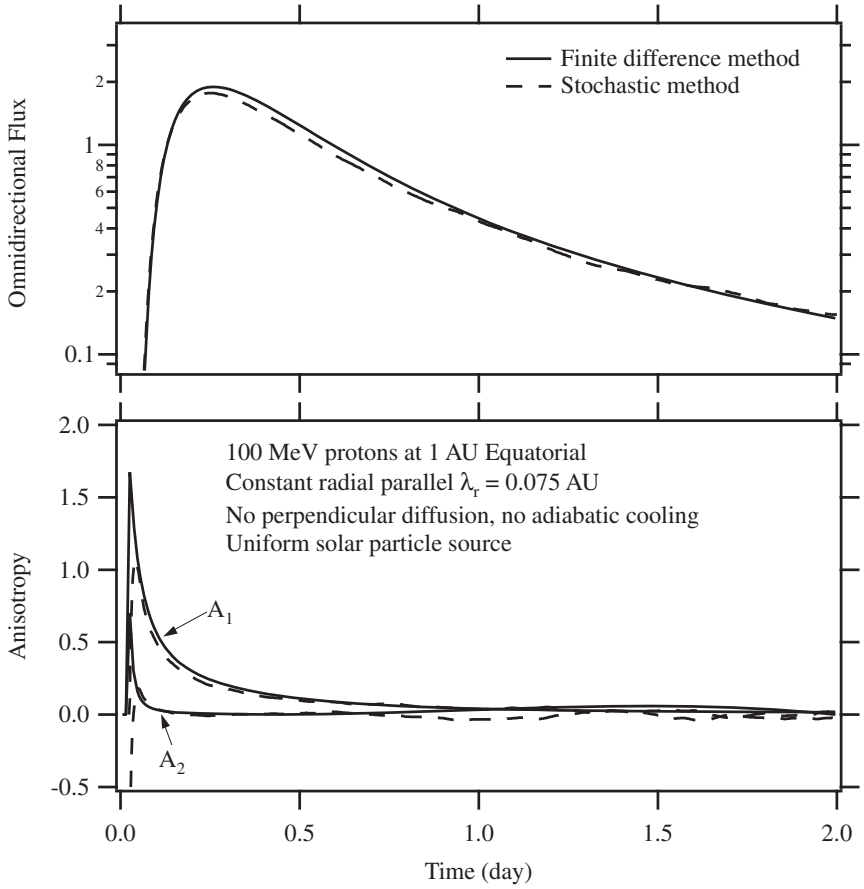

Figure 1. Comparison of calculation results of the focused transport equation using stochastic simulation and finite difference method.

$$A_2 = \frac{f(\mu = 1) - 2f(\mu = 0) + f(\mu = -1)}{f(\mu = -1) + 2f(\mu = 0) + f(\mu = 1)}. \quad (14)$$

As shown in Figure 1, the results of calculation using different computation methods agree within an uncertainty of 5%. The difference probably comes from a different way of calculating the omnidirectional flux and anisotropy used in the finite difference method, which allows finer integration over the full range of the pitch angle. This level of uncertainty will not hinder the application of either of the codes. In addition, in our stochastic code, the calculation is subject to an uncertainty from simulation statistics, which shows up particularly in the late part of an event. With our limited computation power and time, the results presented here are subject to an uncertainty of up to $\sim 10\%$.

3.2. Effect of Adiabatic Cooling on SEP Flux

Figure 2 shows a comparison of calculation runs with and without adiabatic cooling. In these simulations, perpendicular diffusion is still off. We choose a momentum-independent parallel mean free path so that the pure effect of adiabatic cooling can be isolated. As one can see, adiabatic cooling makes a huge difference to the time profile of the SEP flux. The effect becomes apparent even in half a day after the onset. By the time of 1 day, the flux is half of the flux predicted without adiabatic cooling. If we think that particles are lost through leakage to outer heliosphere when no adiabatic cooling is involved, then adiabatic cooling loss of particles greatly dominates the leakage loss. The adiabatic cooling loss effect becomes stronger if the source particle spectrum is more steeply decreasing with momentum. This effect of adiabatic cooling has been discussed in more detail by Qin et al. (2006).

Because of adiabatic energy loss, those particles observed at Earth have less energy than their initial energy at the source. Since the source spectrum steeply decrease with energy, then we will see few particles from higher energies. This is the way how adiabatic cooling affects the SEP flux.

Generally the mean free path is a function of particle momentum. As a result of adiabatic cooling, particles can have different parallel mean free paths on their way from Sun to Earth. Figure 3 shows a calculation of SEP omnidirectional flux and anisotropy with a momentum-dependent parallel mean free path, one with a radial mean free path of $\lambda_r = 0.2$ AU and the other with $\lambda_r = 0.05$ AU at 100 MeV. The omnidirectional flux in the situation of higher parallel mean free path rises to its maximum quickly and then drops down quickly due to fast leakage. First-order anisotropy is larger during the rising phase. In the decay phase, the anisotropy disappears to the levels below our simulation uncertainty due to counting statistics. The flux in the decay phase for the situation of a low mean free path is higher than that of a high mean free path. The fluxes in the both situations decay approximately with the same exponential rate; however, more careful inspection of their ratio (bottom panel in Figure 3) shows that they decay at slightly different rates. The one with higher mean free path decay more slowly, because the particles spend more time at large radial distances where adiabatic cooling is weak. The difference only shows up on the

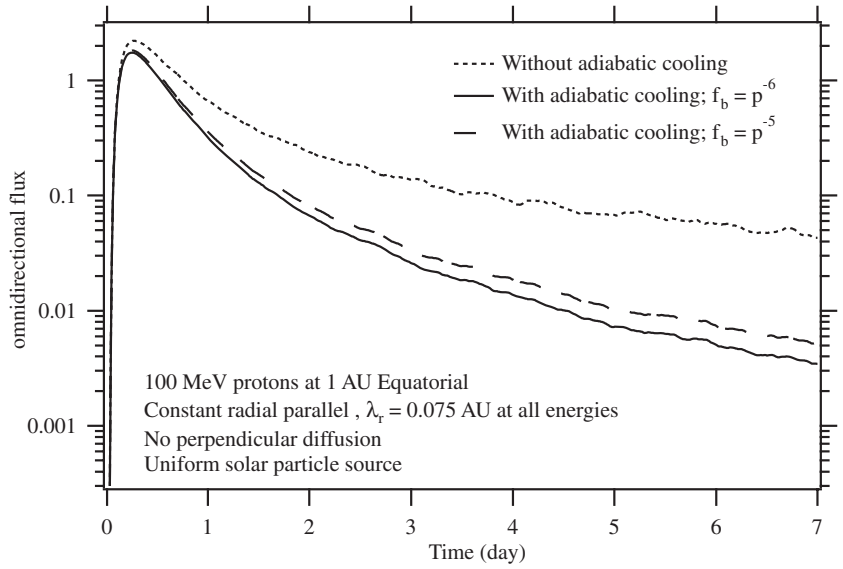

Figure 2. Comparison of omnidirectional flux solved from the transport equation with and without adiabatic cooling.

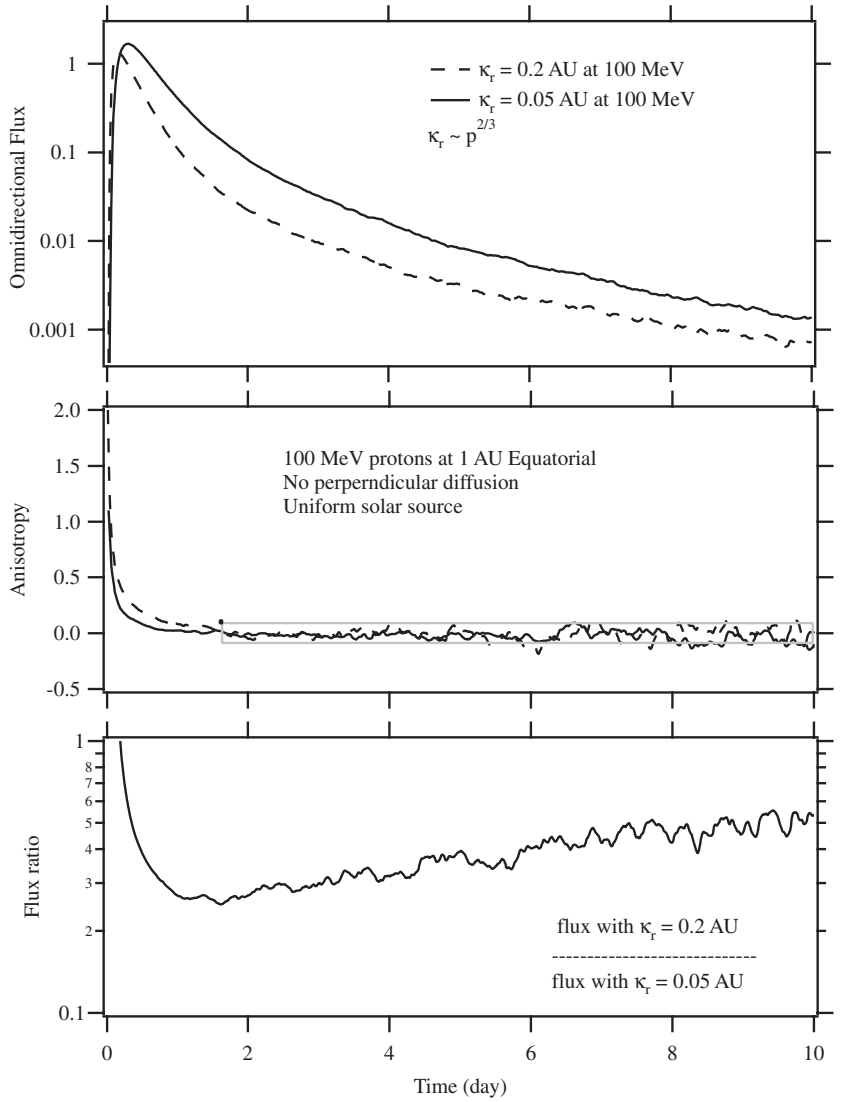

Figure 3. Omnidirectional flux (top), first-order anisotropy (middle) and flux ratio for two different values of parallel mean free path. The rectangular box in the anisotropy panel indicates an estimated uncertainty level of the calculations. Anisotropy below the uncertainty level should be regarded as insignificant anisotropy. Fast small variations in the anisotropy and flux ratio come from statistical fluctuation of flux calculation which does not show up easily in the top panel because of the scale size used.

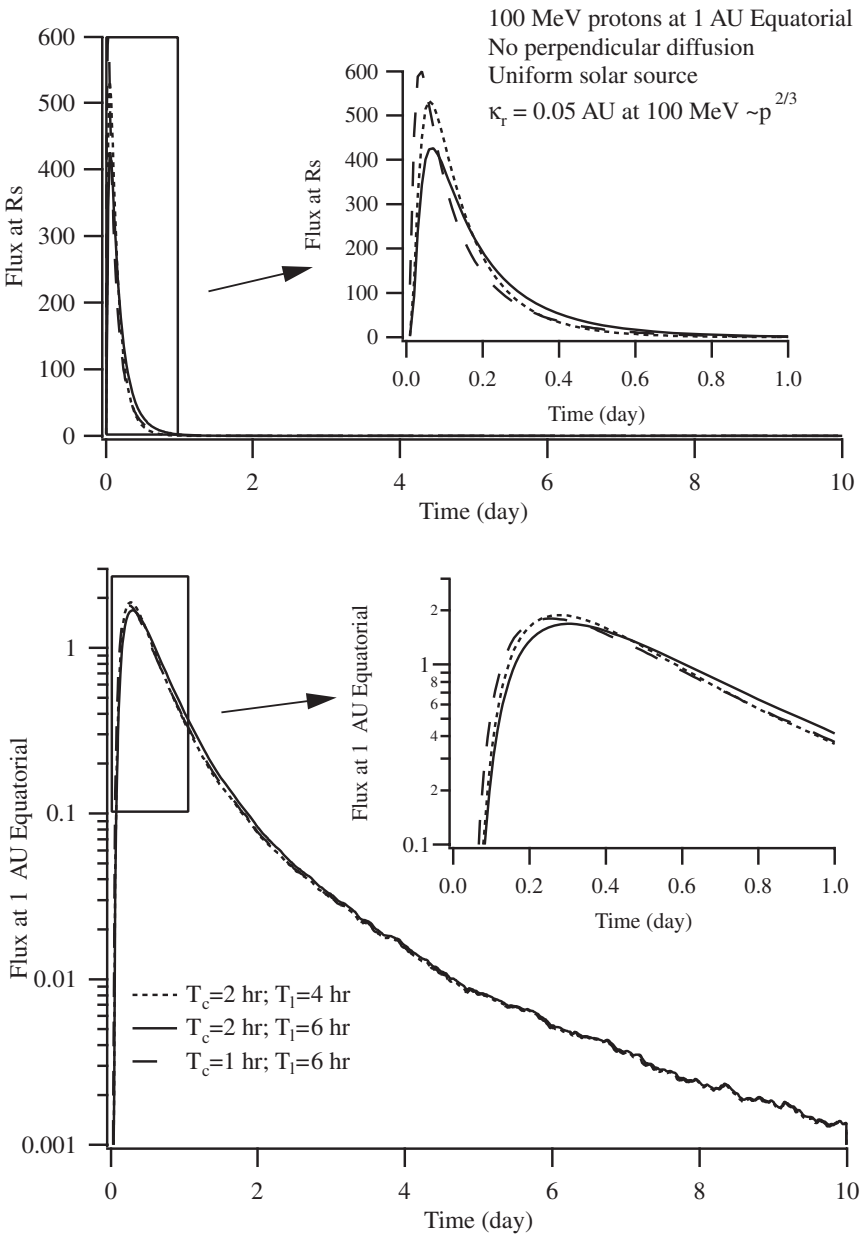

Figure 4. Calculations of omnidirectional flux and anisotropy for three different sets of solar particle injection time profiles.

linear scale, while the fluxes vary on the logarithmic scale. So the rate of flux variation in the decay phase is not sensitive to particle mean free path.

3.3. Effect of Source Injection Profile

Figure 4 shows a comparison of calculations with different source injection profiles. We vary the time constants T_c and T_l in Equation (2) to get different injection time profiles. The total amount of injection is kept constant, i.e., $\int f_b dt = \text{const}$. Although the time duration and peak injection time vary quite bit by several hours and it may affect the time profile of SEP flux and anisotropy in the initial phase of the SEP event (see insertion), the omnidirectional flux as observed at Earth have roughly the same profile over a long period of time. There is a slight difference, but most of them can be compensated by a shift of the main injection time. We have tried the square wave injection profile, the results of the flux time profile remain the same for the long-term behavior. This essentially says that detail of the particle injection profile at the Sun is not important as long as the time of propagation is much longer than the injection period. In a sense, we can model all SEP injection as a δ-injection for long duration events. If it fits observations, the physical implication of this analysis is that most SEPs are injected into the interplanetary medium at the inner boundary all at once. Therefore, in the following presentation we only use one set of time constants for the injection, that is, $T_c = 2$ hr and $T_l = 6$ hr.

3.4. Momentum Distribution of Source Contribution

The reason that adiabatic cooling plays a dominant role in SEP flux can be seen from the investigation of distribution of the source particle. If we bin the values inside the average of Equation (6 or 9) by source particle momentum p_e and transport

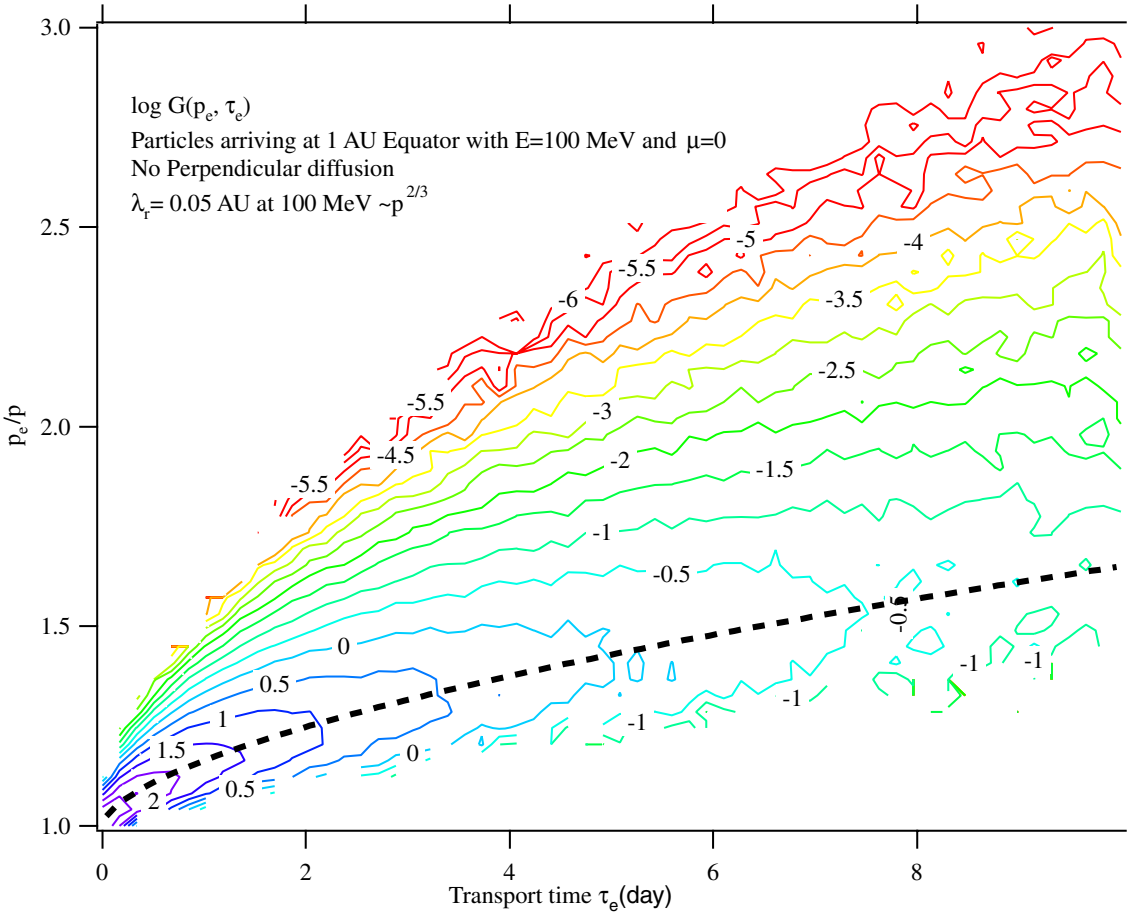

Figure 5. Contour plot of backward Green's function in the logarithmic scale as a function of the transport time and source particle momentum. The dashed line approximately indicates the momentum location at the peak value of Green's function.
(A color version of this figure is available in the online journal.)

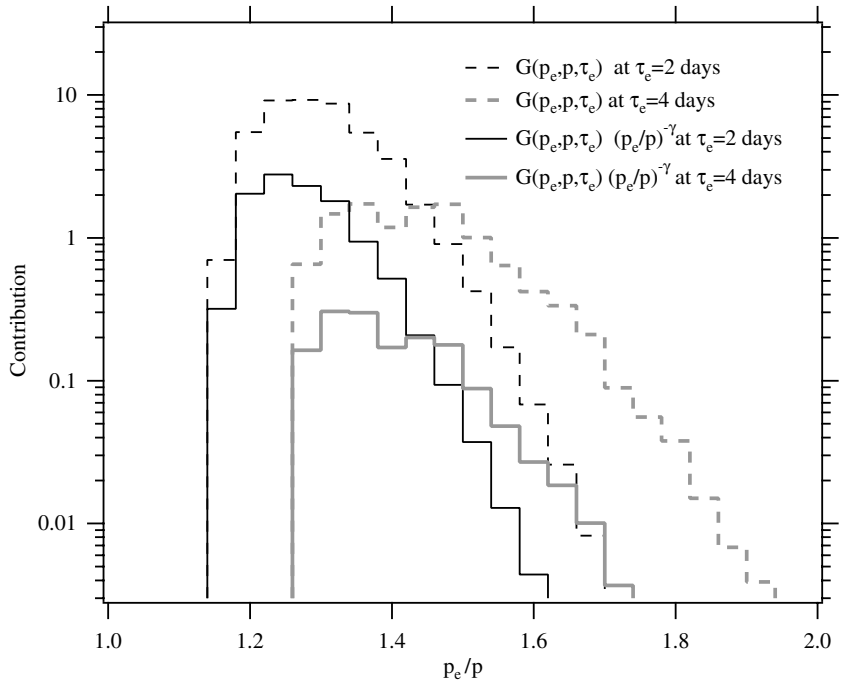

Figure 6. Momentum distribution of source contribution to the solution of the transport equation at two transport time intervals. The dashed lines are not weighted by the source particle spectrum.

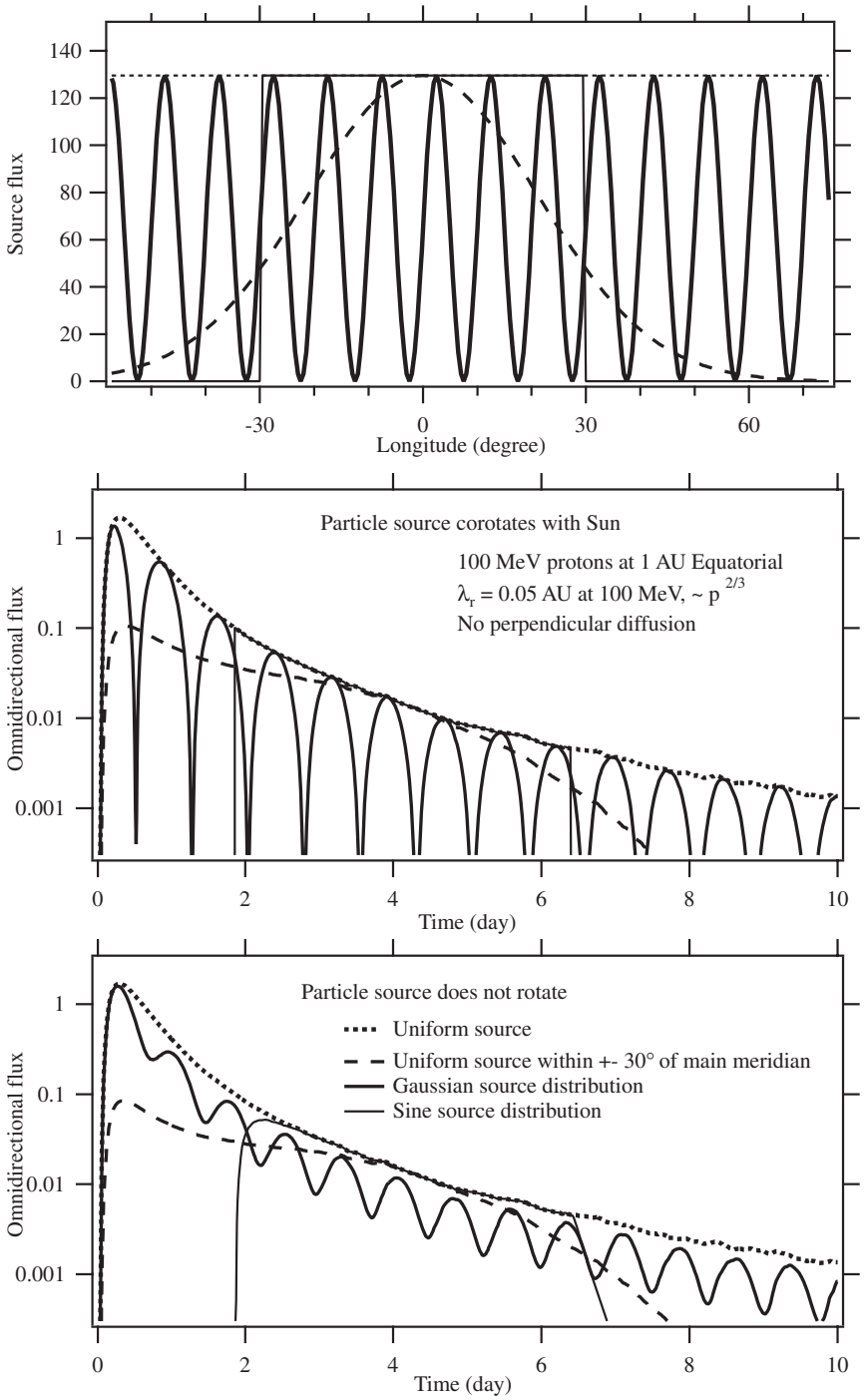

Figure 7. Calculation results of omnidirectional flux with four different longitudinal distributions of solar source particles (top panel) when the perpendicular diffusion is set zero. The solar particle source is set to corotate with Sun in the middle panel and stationary in space in the bottom panel.

time τ_e, then the solution to the transport equation can be written as

$$f(\mathbf{x}, \mu, p, t) = \int G(p_e, \tau_e; \mathbf{x}, \mu, p, t) f_b(\mathbf{x}_e, \mu_e, p_e, t_e) d\tau_e dp_e, \quad (15)$$

where $G(p_e, \tau_e; \mathbf{x}, \mu, p, t)$ can be viewed as a backward Green's function. The simulation of stochastic processes is ideally designed to find Green's function. Figure 5 displays a contour plot of $\log G(p_e, \tau_e; \mathbf{x}, \mu, p, t)$ for protons arriving at Earth with 100 MeV energy and $\mu = 0$ as a function of source momentum p_e/p and transport time τ_e. It is homogeneous in the time t because we have used a steady state interplanetary medium and magnetic field. $G(p_e, \tau_e; \mathbf{x}, \mu, p, t)$ is strongly peaked at some momentum values approximately located along the dashed line.

The product $G(p_e, \tau_e; \mathbf{x}, \mu, p, t) f_b(\mathbf{x}_e, \mu_e, p_e, t_e)$ is the true distribution of source particles for those observed at $\mathbf{x}$, μ, p, and t. Since the boundary value $f_b(\mathbf{x}_e, \mu_e, p_e, t_e)$ depends on t through $t_e = t - \tau_e$, the entire solution is time dependent. Weighted by the shape of the source particle spectrum f_b in Equation (2), the source particle distribution will be shifted to slight lower momentum because of steeply decreasing the source spectrum. Since the boundary value is strongly peaked

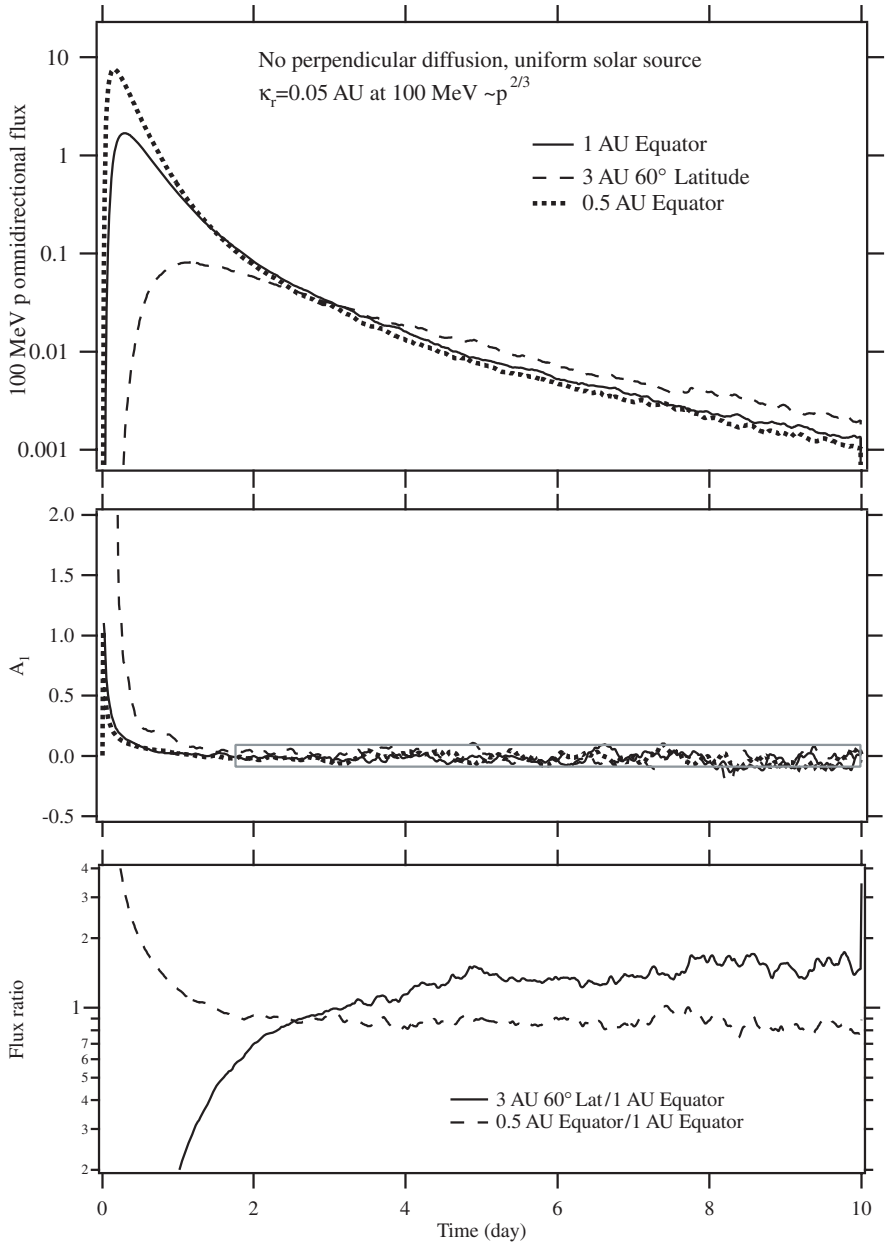

Figure 8. Comparison of 100 MeV proton omnidirectional flux and anisotropy at three different locations in the heliosphere. The solar particle source is uniform as a function of latitude and longitude. The calculations use a low value for the parallel mean free path. Anisotropy values in the rectangular box are not significant.

within a short $\sim T_l - T_c$ time from $t_e = t - \tau_e = 0$, only those trajectories that fall into the inner boundary within a narrow time window makes a major contribution to the calculation of particle flux. Inside this window, the distribution $G(p_e, \tau_e; \mathbf{x}, \mu, p, t) f_b(\mathbf{x}_e, \mu_e, p_e, t_e)$ as a function of p_e reflects the actual momentum distribution of source particles. Figure 6 displays this distribution of particles arriving at 2 days and 4 days after event onset as a function of particle momentum at the source. They are obtained from the simulation of stochastic trajectories that fall within a 4 hr window at those transport time intervals. These are absolute values of the contribution to the solution of transport equation. The contribution becomes much lower when a more steeply decreasing spectrum is introduced, which indicates the importance of the adiabatic cooling effect. Particles arriving at later time come from Sun with higher momentum and lower intensity. That is the major mechanism for the dissipation of SEPs during the decay phase.

3.5. Time Profile of SEP Flux and Anisotropy at Different Locations

3.5.1. Without Perpendicular Diffusion

If particles do not cross field line, particles observed at different locations and time can come from completely different source populations. So the assumption about the longitudinal and latitudinal distribution of SEP sources can severely affect the SEP flux time profiles observed by any spacecraft. Figure 7 demonstrates SEP profiles at Earth with four different longitudinal distributions of source strength $a(\theta, \phi)$: uniform, step wave, Gaussian, and sinusoidal wave oscillation. Some of the distributions are highly hypothetical, but they are mainly used

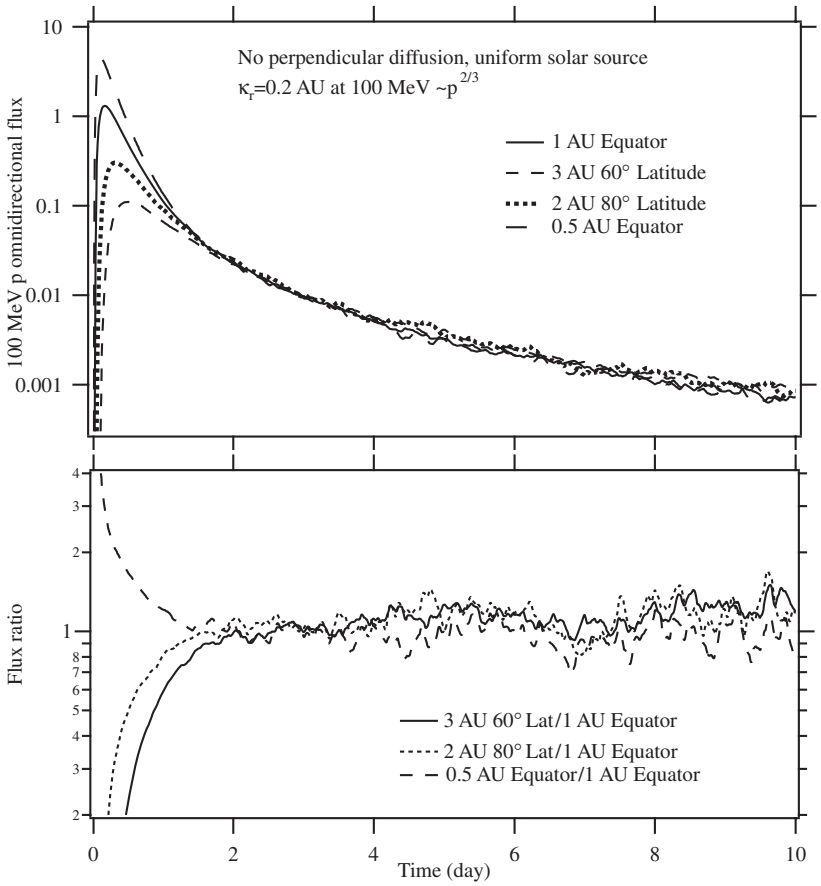

Figure 9. Comparison of 100 MeV proton omnidirectional fluxes at four different locations in the heliosphere. The solar particle source is uniform as a function of latitude and longitude. The calculations use a high value for the parallel mean free path.

to test its sensitivity. In one set (middle panel), we assume that the source is corotating with Sun, while in the other (bottom panel) the source is located at some longitudes in a fixed reference frame. In both cases, the observer at 1 AU Equator is stationary at 0° longitude. The calculation results from these two sets of longitudinal source distributions are a little different, but qualitatively they tell the same story. Essentially the time profile of the SEP flux at Earth preserves the signature of the source longitudinal distribution. In order to apply the calculation to real observations, one then has to make an assumption about the source longitudinal distribution. All the previous models with only particle transport along magnetic field lines suffer this limitation. However, the anisotropy is the same as shown in Figure 3. Significant anisotropy only appear in the first few hours of the event, and it is not necessarily correlated with the ramping-up of the flux, as the flux can be modified by the longitudinal distribution of source strength. The source distribution does not affect the time profile of anisotropy, which can then be used to determine the property of interplanetary transport, such as parallel mean free path, with greater confidence. At least, the anisotropy can be used as an indication to tell whether an observer is directly connected to the source at the initial injection time.

Now let us compare the time profiles of SEP event observed at different locations in the heliosphere. Figure 8 shows the omnidirectional flux of 100 MeV protons and first-order anisotropy at 1 AU Equator, 3 AU 60° latitude, and 0.5 AU Equator. The source particle strength on the Sun is uniform over all latitude and longitude. The flux levels in the early phase of the event at the three locations are very different, and the peak fluxes can differ by almost 2 orders of magnitude. The closer is the observer to the Sun, the larger is the peak flux. This is mainly due to the geometric factor of $1/r^2$, but it is not exact because of scattering. But after 2 days into the event, the flux levels at the three different locations reach almost the same within a factor two. This behavior is very close to what have been observed by experiments as the reservoir phenomena, except the decay rates of the SEP flux at the three locations are slightly different, particularly that at 3 AU. The ratio of the omnidirectional fluxes at 3 AU to 1 AU increases with time but in a very slow pace, indicating that the flux at 3 AU decays more slowly than at 1 AU. It happens because of less adiabatic cooling at larger radial distances. Significant anisotropies appear only in the initial phase when the flux is rising. The anisotropy and omnidirectional flux at 3 AU appear delayed, an effect purely coming from scattering over a larger distance. A naive analysis of flux onset as observed at large radial distances may result in a wrong conclusion about the onset of solar event and source particle injection time.

If we increase particle mean free path, the fluxes at all four different locations in Figure 9 reach a uniform level in less time as short as 2 days. Difference of flux levels in the decay phase is no more than 50%, which is a very good consistency given the fact the SEP flux can vary over several orders of magnitude at the peak of an event. The consistency probably can be better than 50% if we make more accurate runs with better statistics. The observed reservoir phenomenon may be explained in this way. The only requirement here is that the source

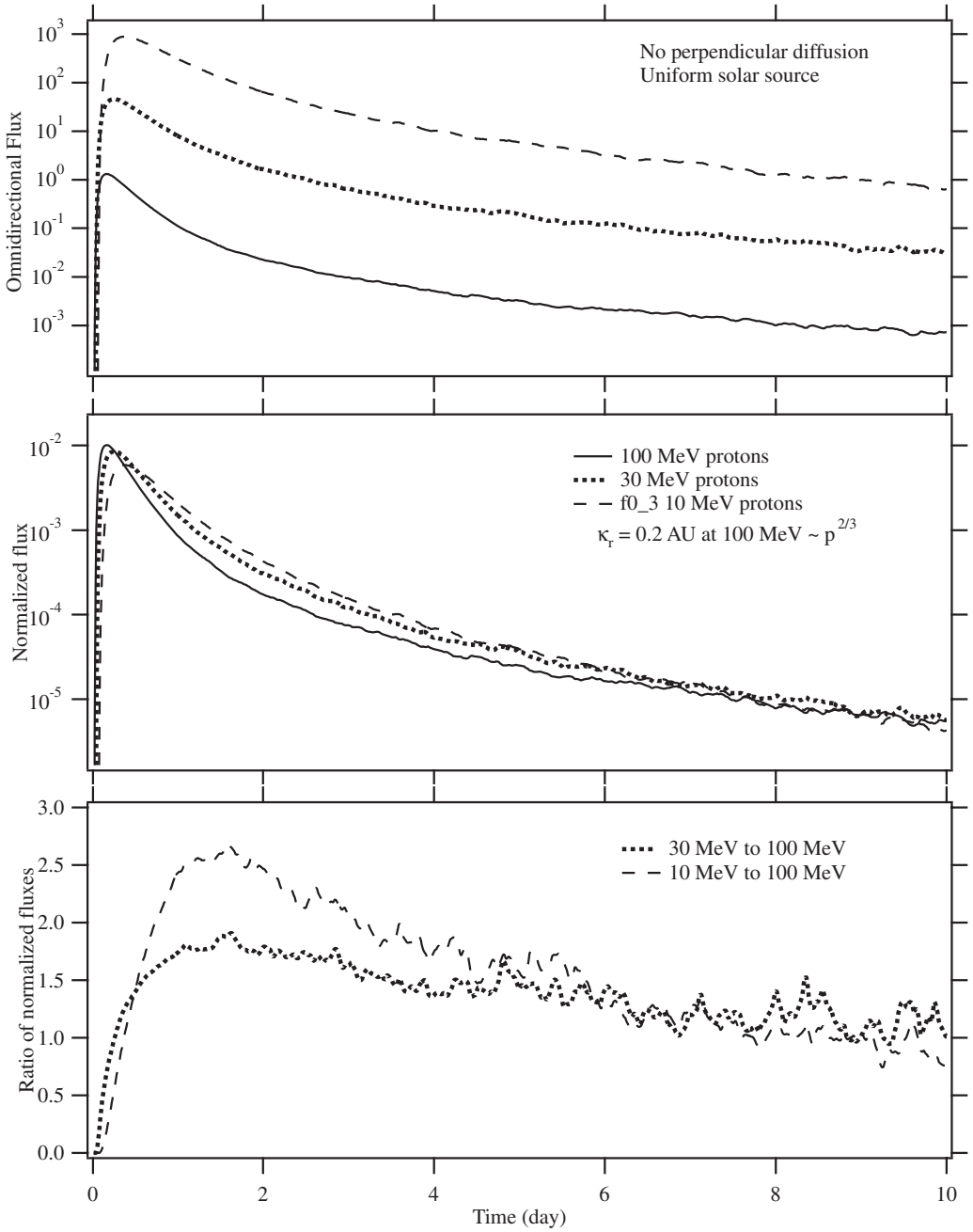

Figure 10. Comparison of omnidirectional flux at three different energies at 1 AU Equator. The normalized flux is the flux divided by source intensity at its corresponding energy. The solar particle source is uniform as a function of latitude and longitude. Perpendicular diffusion is set to zero. The calculations use a high value for the parallel mean free path.

particle strength is uniform over the entire solar longitudes and latitudes.

If we allow the source particle injection strength to vary considerably with the solar longitude and latitude, in a model without perpendicular diffusion the SEP fluxes will never reach a nearly uniform level. The difference in the slow decay phase will be proportional to the difference of the total number of particles injected on different field lines. So comparison of SEP fluxes at different locations in the heliosphere with a nonuniform solar source becomes complicated or perhaps even meaningless because the calculation results depend too arbitrarily on the longitudinal and latitudinal distribution of source strength on the Sun. If we want to insist no cross-field transport, some other constraints must be assumed in order to apply any calculation to multispacecraft observations. Such a requirement is more strict if one wants to compare observations at different latitudes, because interplanetary field lines in the Parker model do not mix across latitude.

Figure 10 shows the omnidirectional fluxes for particles observed at Earth with three different energies. The particles have different mean free paths according to the prescribed momentum dependence in Table 1. At glance, the three flux curves are almost parallel to each other in the decay phase. However, more close inspection with the fluxes normalized to their source injection strengths find that there are small differences in the decay rate. The differences are more obvious if the mean free path is smaller (Figure 11). Generally, the smaller the parallel mean free path is, the faster

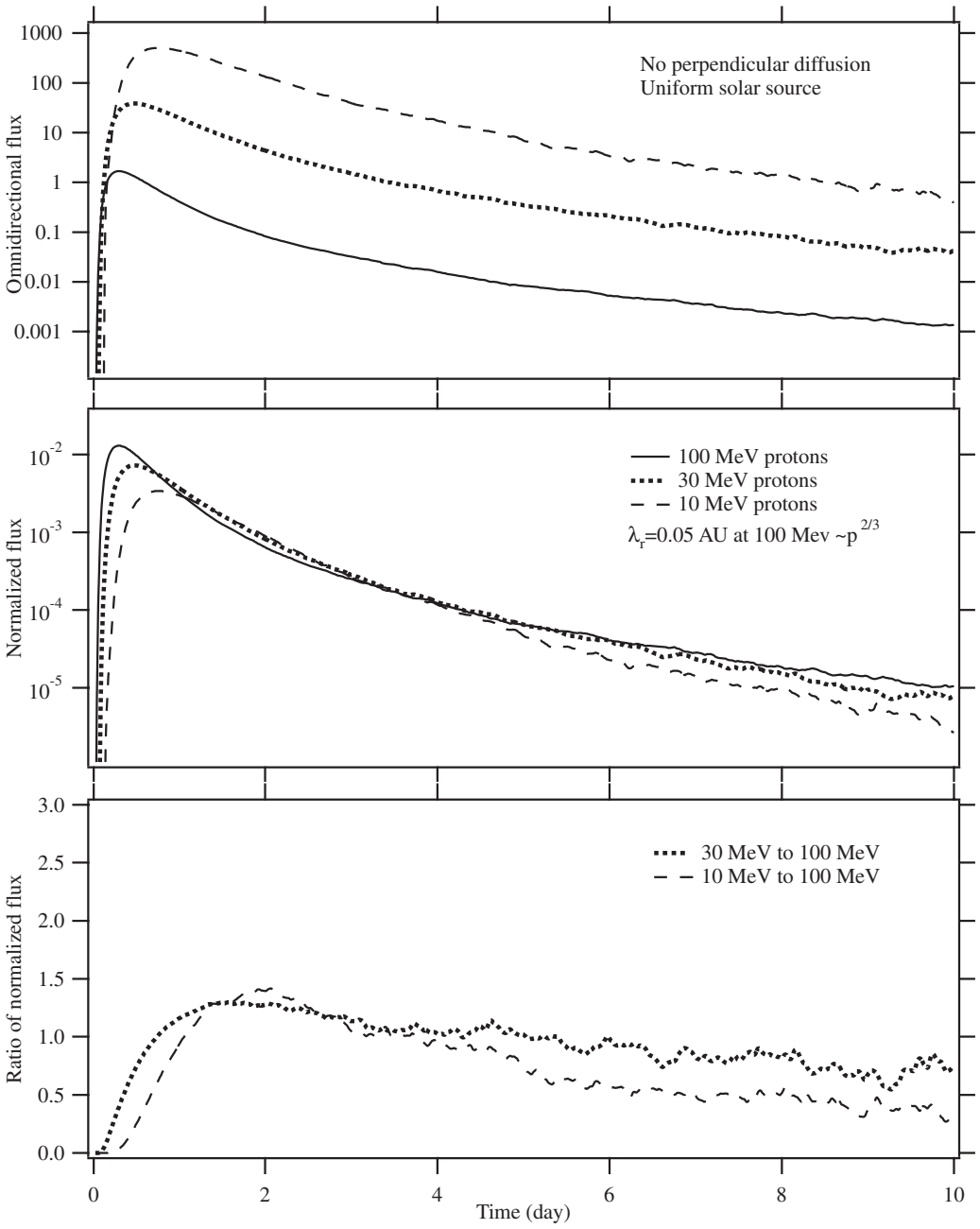

Figure 11. Same as Figure 10 except a low value is used for the parallel mean free path.

the flux decay, which is consistent with the pictures from Figure 3.

Figure 12 shows the trajectory of a sample stochastic process in the equatorial plane. The trajectory follows an outward propagating magnetic field line back and forth several times before reaching its final destination at 1 AU. The total propagation time is 1.78 days for this trajectory. The trajectory reaches as far out as $\sim$ 2.5 AU and most time is spent close to the Sun. The trajectory shows a reason why we see the nearly inform flux throughout the inner heliosphere in the decay phase after the particles have had chance to go almost everywhere in the inner heliosphere. Since the decay of SEP flux is mainly through adiabatic cooling and cooling is strongest near the Sun, those particles with smaller mean free path are more confined thus losing momentum faster. In addition, we found from the tracing of trajectory that average behavior of the adiabatic cooling rate is slightly different from the isotropic formula $dp/dt = -\nabla \cdot \mathbf{V}_{sw} p/3$ even though the pitch-angle diffusion is very rapid. This suggests that the Parker transport equation is not adequate in describing the propagation of SEPs in the inner heliosphere.

3.5.2. With Perpendicular Diffusion

Now we turn on particle diffusion across magnetic field lines with a perpendicular diffusion coefficient typically used in cosmic ray modulation study. Figure 13 shows a comparison of the SEP fluxes at Earth and 3 AU high latitude with and without perpendicular diffusion. The source distribution is still uniform as a function of latitude and longitude on the Sun. Although small, the difference exists. The difference mainly comes from leakage of particles to the outer boundary through perpendicular diffusion at large radial distances.

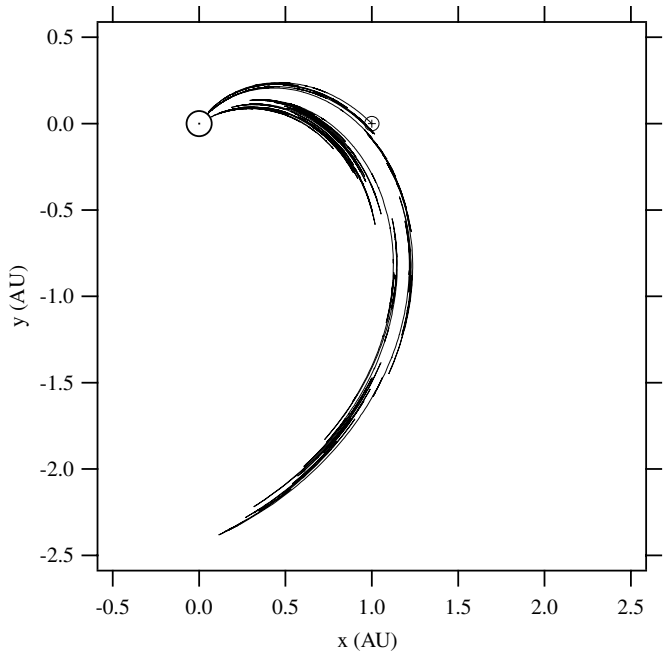

Figure 12. Sample trajectory in the equatorial plane. The trajectory starts from the Sun and arrives 1 AU Equator at 0 longitude. Gray shade level of the curve indicate the momentum.

Figure 14 shows a comparison of SEP flux time profiles at Earth and 3 AU 60° latitudes. The source on the Sun is uniform and perpendicular diffusion is on. Compared with the same calculations without perpendicular diffusion in Figure 8, the flux with perpendicular diffusion becomes more uniform, as the ratio of the SEP omnidirectional flux at 1 AU to that at 3 AU is very close to 1 and the same ratio persists throughout the decay phase after ~ 4 days. The first-order anisotropy remains approximately the same behavior as in Figure 8, so it is not shown here. The conclusion we can reach here is that the perpendicular diffusion improves the uniformity of the reservoir.

(A) Effects of the longitudinal distribution of source particles. Now let us look at a situation where the source on the Sun is function of longitude. Figure 15 shows 100 MeV proton omnidirectional fluxes at 1 AU Equator and several longitudes that have different magnetic connections to a solar source of 90° wide in longitude and 180° wide in latitude. As a reference, the time profile of the omnidirectional flux from a uniform solar source is shown by the light gray curve. If an observer is directly connected to the source at the onset of the event, the initial phase of the SEP event is very much the same as from the uniform solar source (dotted line). As time progresses, the observer moves out of direct connection to the source and the flux decays faster than from a uniform source. There is no sudden change of particle flux or decay rate when it is disconnected from the source. This is a major difference that perpendicular diffusion

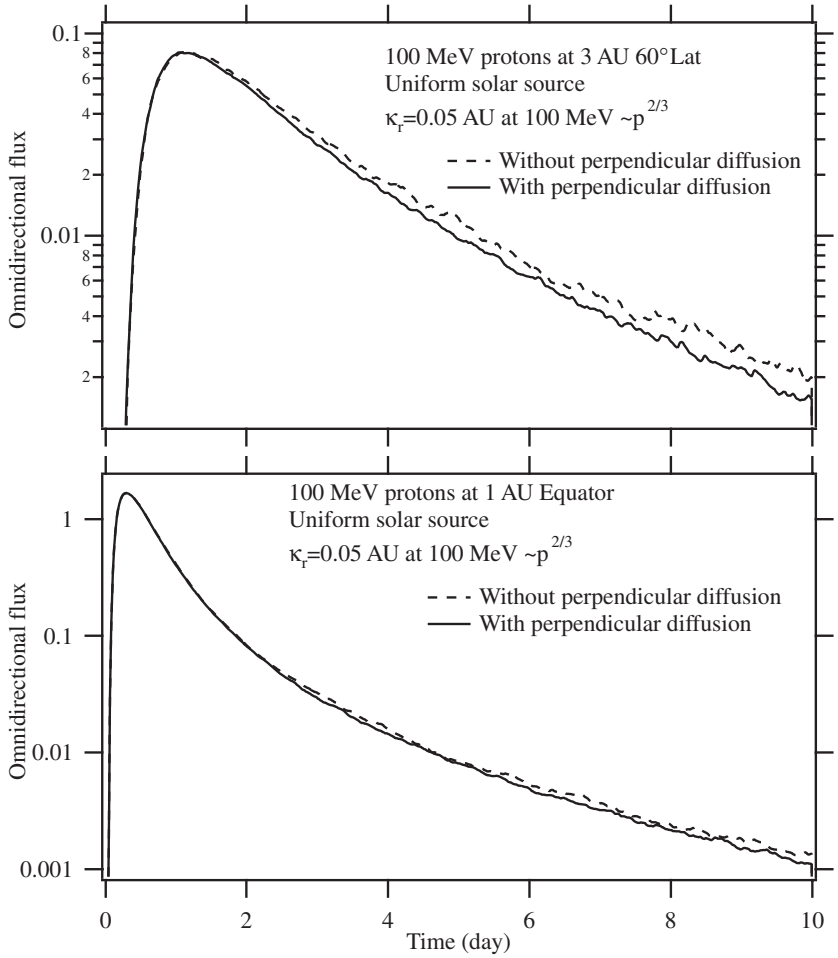

Figure 13. Comparison of omnidirectional fluxes with and without perpendicular diffusion. The solar particle source is uniform as a function of latitude and longitude. The calculations use a low value for the parallel mean free path and perpendicular diffusion coefficient.

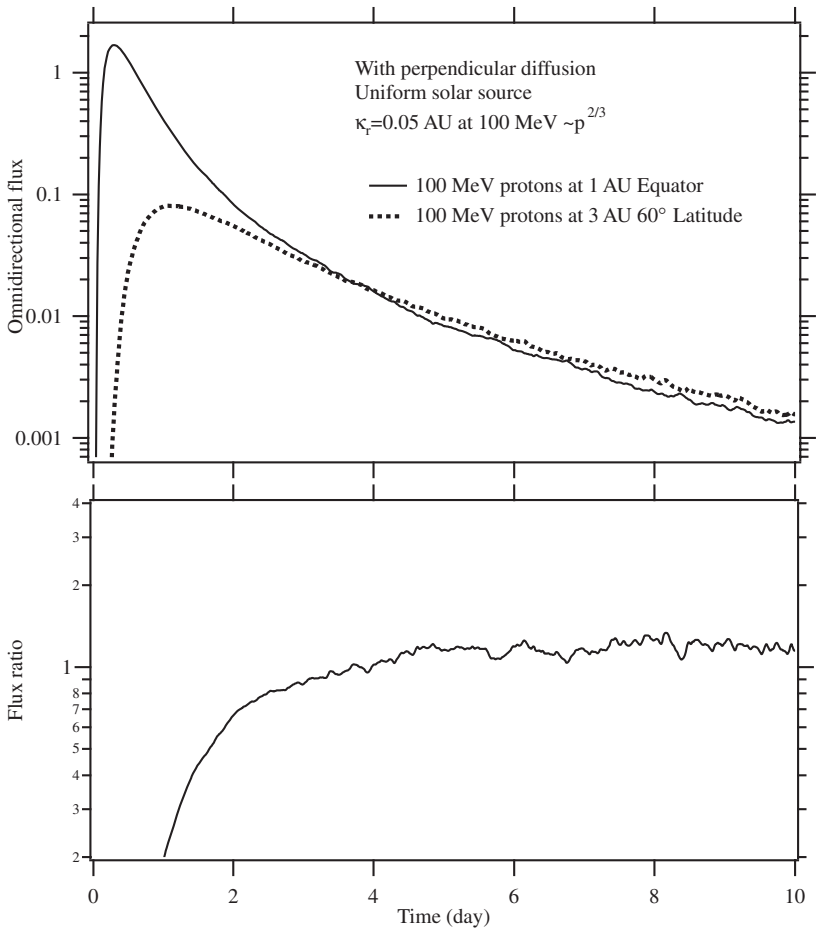

Figure 14. Comparison of omnidirectional fluxes at two different locations in the heliosphere when perpendicular diffusion is turned on. The solar particle source is uniform as a function of latitude and longitude. The calculations use a low value for the parallel mean free path and perpendicular diffusion coefficient.

makes. When the observer is not directly connected to the source on the Sun initially, the increase of SEP flux is delayed. The amount of delay depends on how great the separation of the field line is from the field lines directly connected to the source. Particles are observed no matter whether it is connected to the source or not. The flux levels and amount of time delay may show a huge dependency on the magnetic connection. But the differences diminish as time progresses. By the end of the plot (10 days), the difference is more than a factor of 3 for this set of parameters. The behavior of anisotropy is essentially unaffected by magnetic connection, that is, large enough anisotropy only shows up in the initial phase and it is not correlated with flux increase. So anisotropy again can be used to judge weather the observer is directly connected to the source at the onset of an event (not the onset of SEP flux). Figure 16 shows our calculations of omnidirectional flux and anisotropy at 3 AU 60° latitude for various longitudinal connection to the source. The story remains essentially the same as at 1 AU, except that the differences due to longitudinal locations are smaller. It means that longitudinal inhomogeneity of SEP flux is less at larger radial distances and high latitudes. The reason is probably from the geometry of Parker spiral: at large radial distances from the Sun the spatial separation of field lines from different longitudes approach a constant while perpendicular diffusion is getting larger, resulting in a more efficient longitudinal diffusion at larger radial distances.

If we increase the transport coefficients, both parallel and perpendicular, we get Figures 17 and 18. The difference due to longitudinal separation of field lines to the solar source location gets much smaller than in Figures 15 and 16. At 3 AU the flux is almost uniform after 4 days into the event, while at 1 AU a uniform flux is reached a little later.

Figure 19 shows a comparison of calculation results with a uniform source and one with sinusoidal longitudinal source variation as shown in Figure 7. The perpendicular diffusion essentially has completely smoothed out all the longitudinal variations of source strength. There is a factor of 2 difference of the intensity in the decay phase simply because the sinusoidal wave source injects half as much as the uniform source.

(B) Effects of latitudinal distribution of source particles. Let us now look at SEP from a solar source that has a limited coverage of solar latitude. In Figure 20, we show SEP fluxes from a solar source that covers a 90° wide cone angle. One source (top panel) is centered at the footpoint of the magnetic field line connecting to one of the observers located at 1 AU Equator. The other observer is located at 3 AU 60° latitude. Both locations are connected to the same longitude on the Sun. Apparently, the omnidirectional fluxes at the two locations have not reached the same level within 10 days, although they are approaching each other with a difference less than a factor of 2 at the end of the plot. If we move the center of the solar source to the magnetic footpoint of the observer at 3 AU 60° latitude, the flux at 3 AU becomes much higher than at 1 AU and the fluxes do not seem to approach a uniform level. Even though we put a high value for the transport coefficients in Table 1, the differences still remain as shown in Figure 21. This

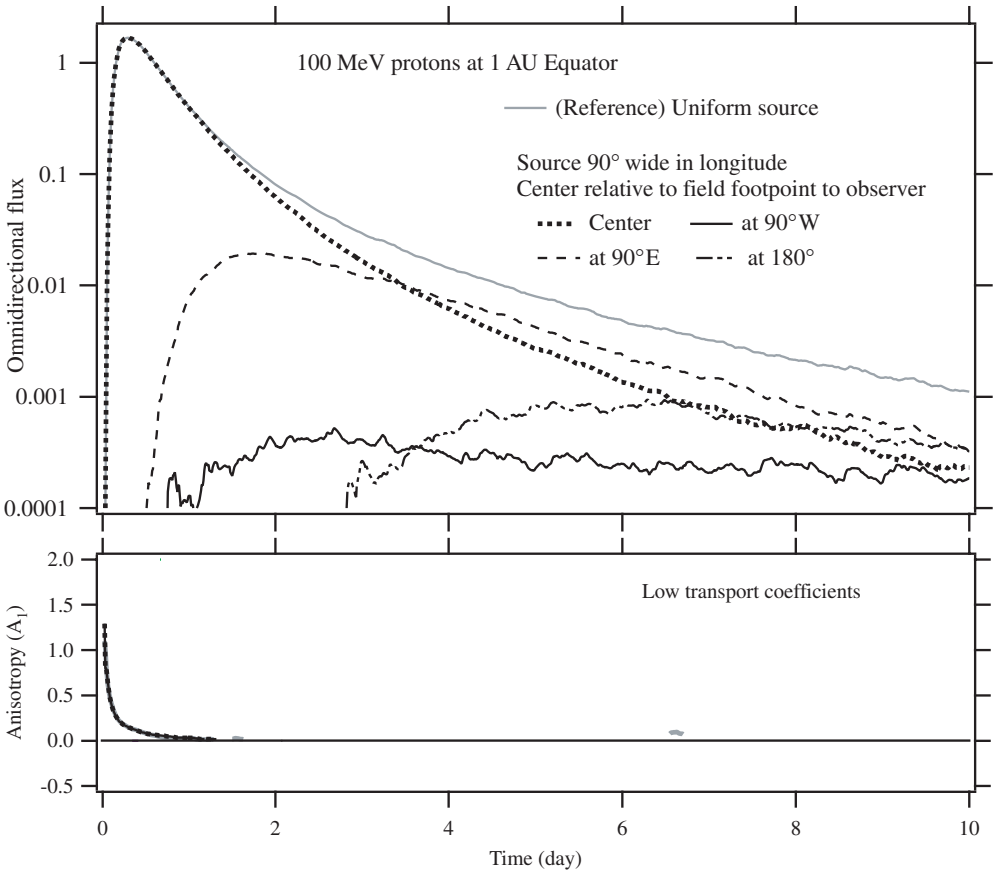

Figure 15. Omnidirectional flux and anisotropy at four different longitude locations at 1 AU Equator. The solar particle source is uniform in latitude, but only covers 90° in longitude. The calculations use a low value for the parallel mean free path and perpendicular diffusion coefficient.

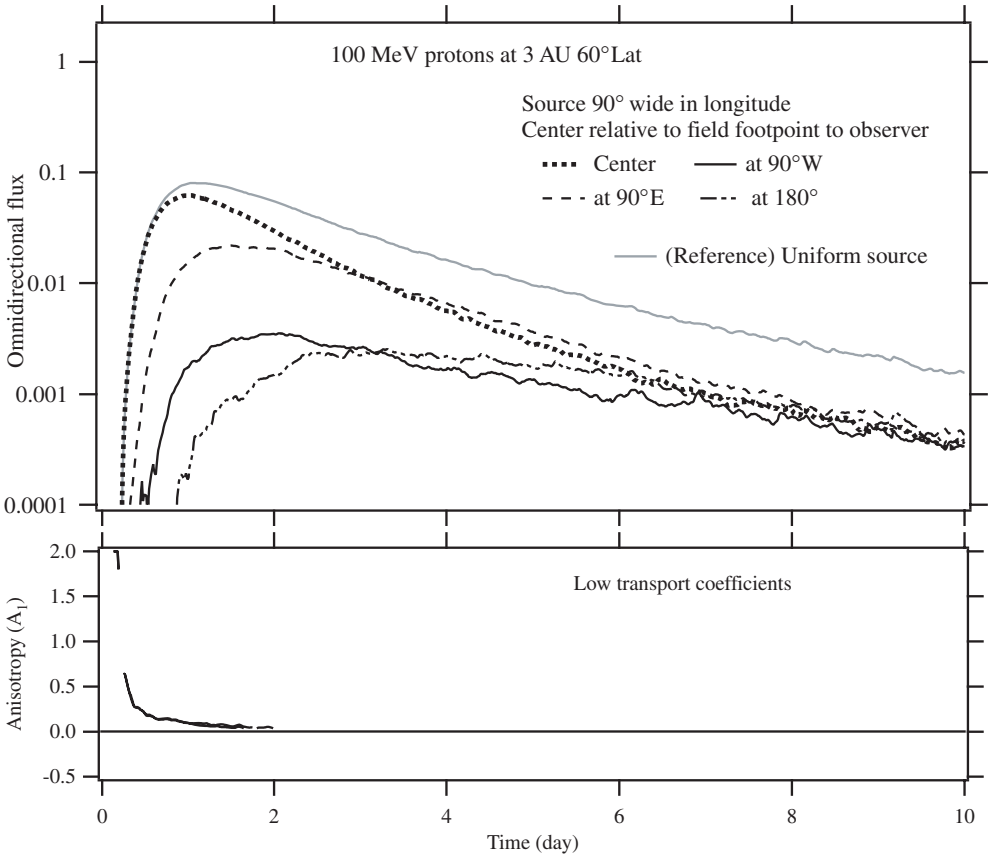

Figure 16. Same as Figure 15 for four longitudes at 3 AU 60° latitude.

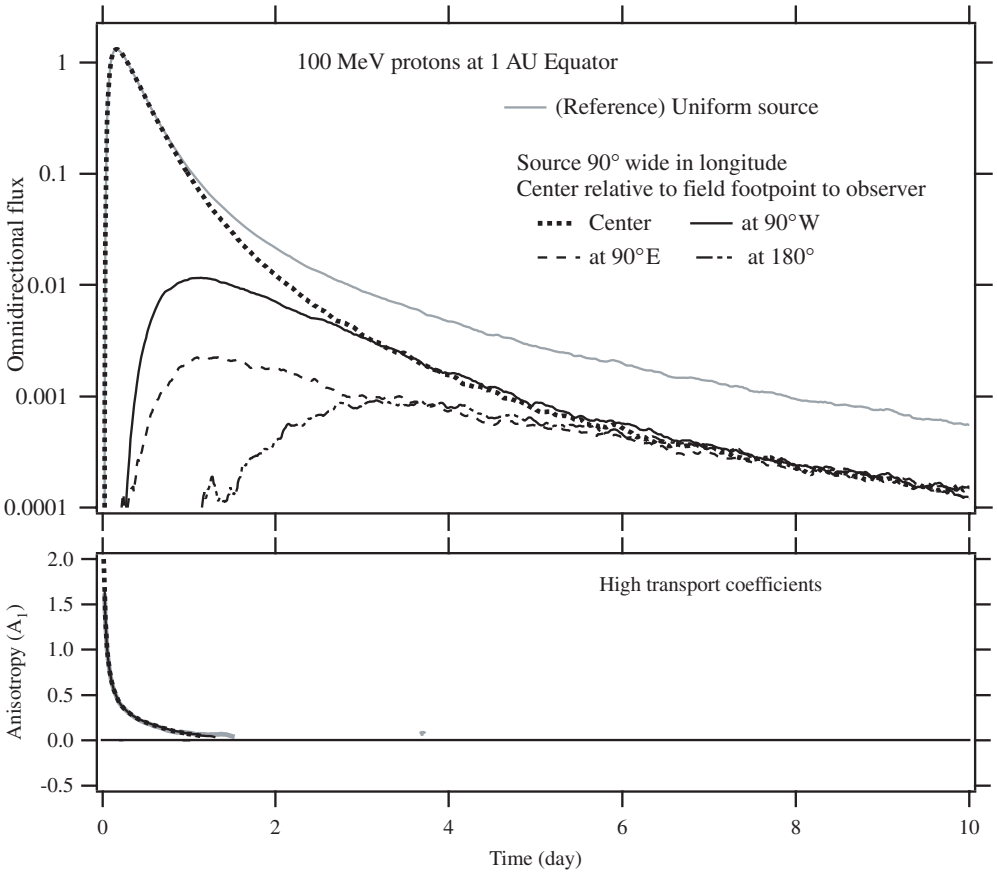

Figure 17. Same as Figure 15 for a high value of parallel mean free path and perpendicular diffusion coefficient.

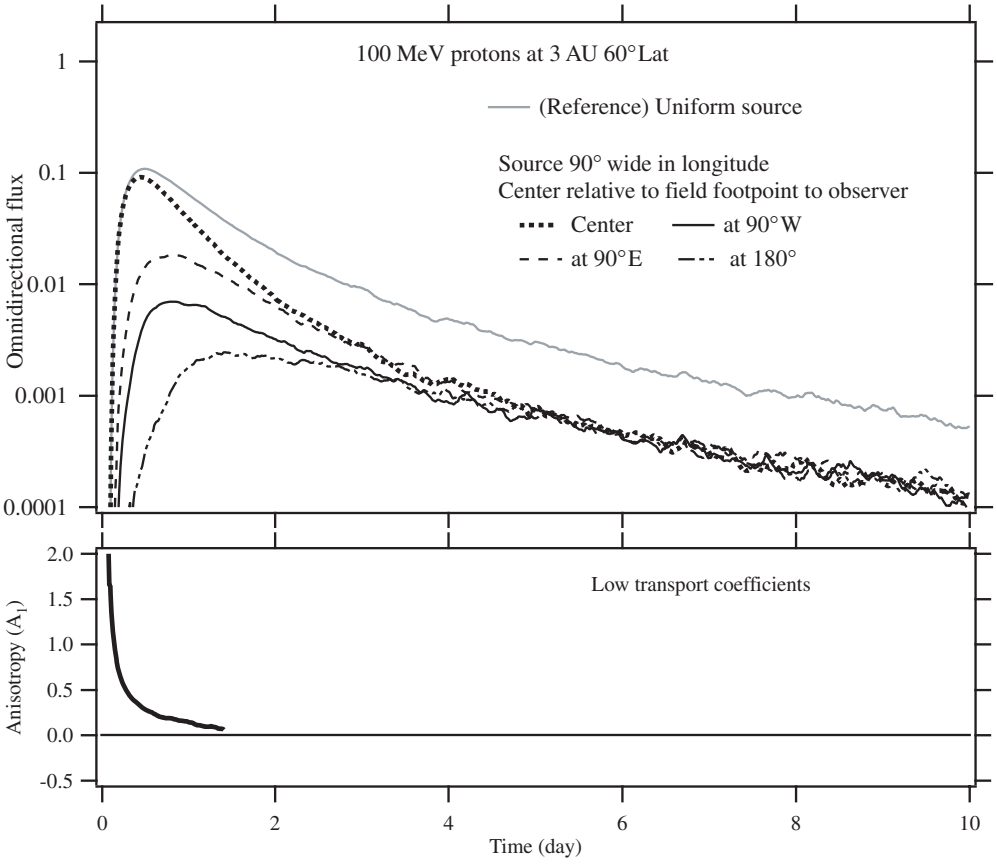

Figure 18. Same as Figure 16 for a high value of parallel mean free path and perpendicular diffusion coefficient.

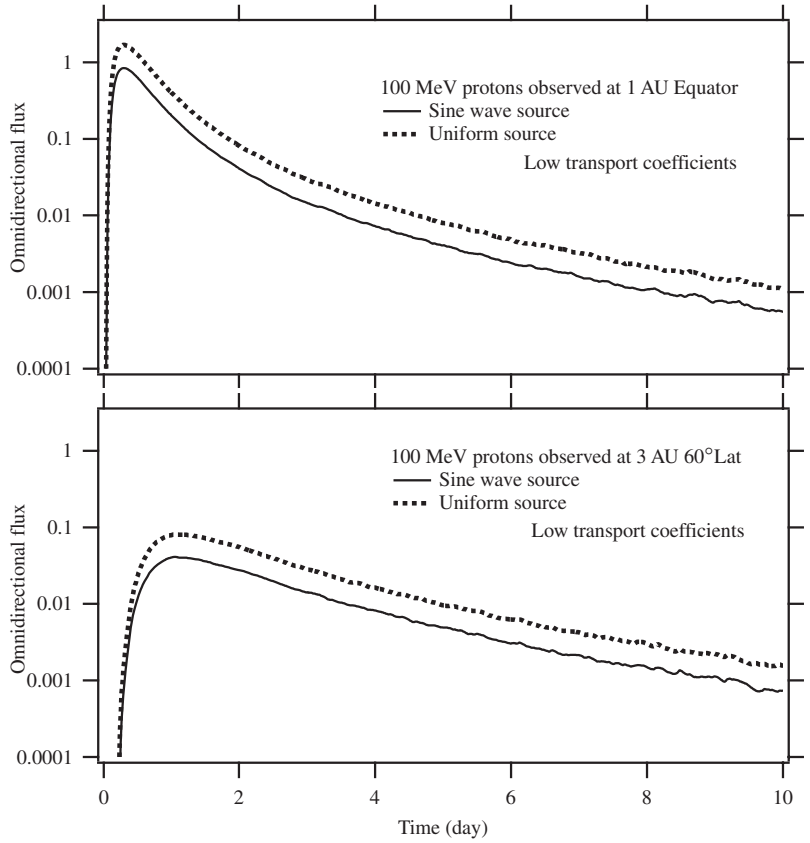

Figure 19. Comparison of omnidirectional flux from a uniform solar source and that from a source with a sinusoidal wave longitudinal variation.

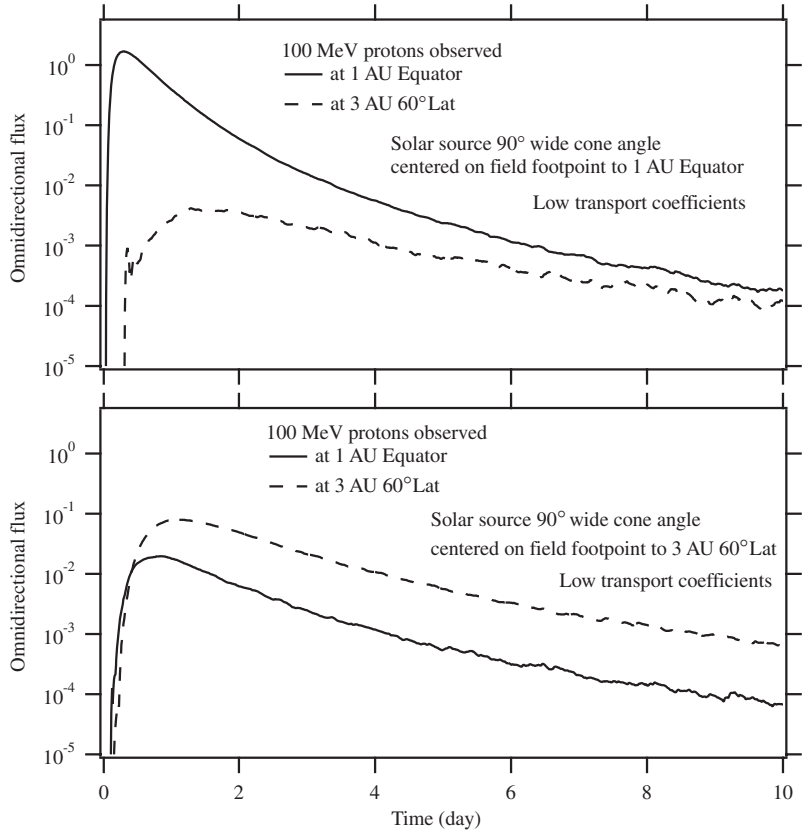

Figure 20. Omnidirectional fluxes at two locations from a solar source that covers a 90° cone angle on the Sun. The calculations use a low value for the parallel mean free path and perpendicular diffusion coefficient.

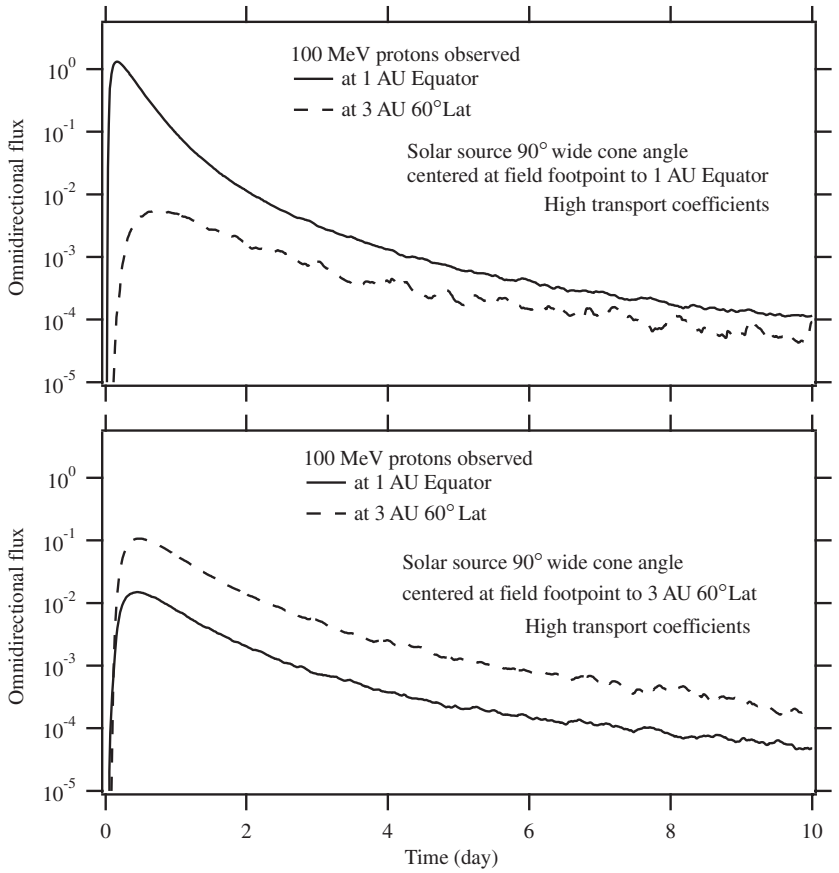

Figure 21. Same as Figure 20 when a high value is used for the parallel mean free path and perpendicular diffusion coefficient.

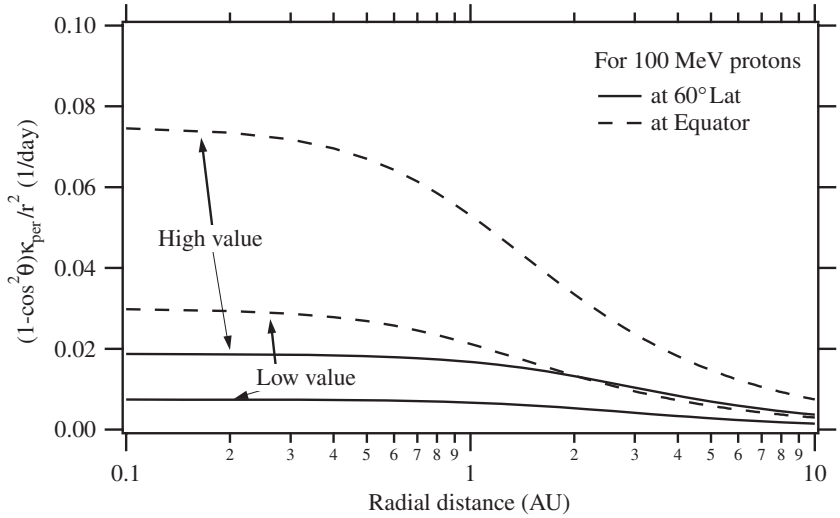

Figure 22. Diffusion coefficient in cosine of colatitude used in this calculation as a function of radial distance and latitude.

calculation result indicates that the prescribed perpendicular diffusion is not high enough to make the particles diffuse across the large range of latitudes. This behavior is different from the behavior in the longitudinal direction shown above. The result is sort of expected because the spatial dependence of the perpendicular diffusion given in Table 1 corresponds to a diffusion in cosine of colatitude $(1-\cos^2\theta)\kappa_\perp/r^2$ that decreases with radial distance (Figure 22) and most of latitudinal transport occurs close to the Sun, but our given level of perpendicular diffusion is still not enough. As a reference, the latitudinal diffusion in cosine of colatitude needs to be ~ 1 day^{-1} in order for the particles to diffuse over the entire latitude range in a few days.

Figure 23 shows the ratios of perpendicular to parallel diffusion coefficients used in this calculation. In order to reproduce a latitudinal uniformity of SEP fluxes, we need to increase perpendicular diffusion. Enhancement of latitudinal transport has been inferred from Ulysses observations of cosmic rays and energetic particles accelerated by corotating interaction regions at high latitudes (Kota & Jokipii 1995; Potgieter et al. 1997). The question here is how much increase we can put in so that it is still consistent with observations of comic

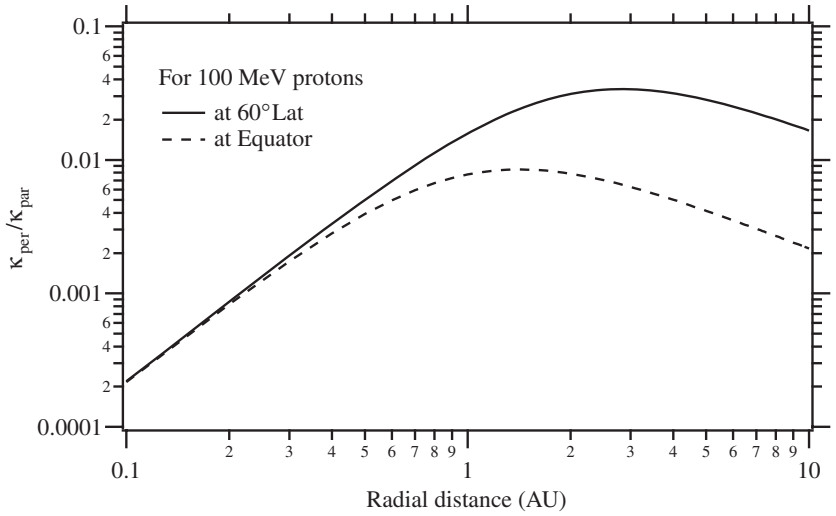

Figure 23. Ratio of perpendicular to parallel diffusion coefficients used in this calculation as a function of radial distance and latitude.

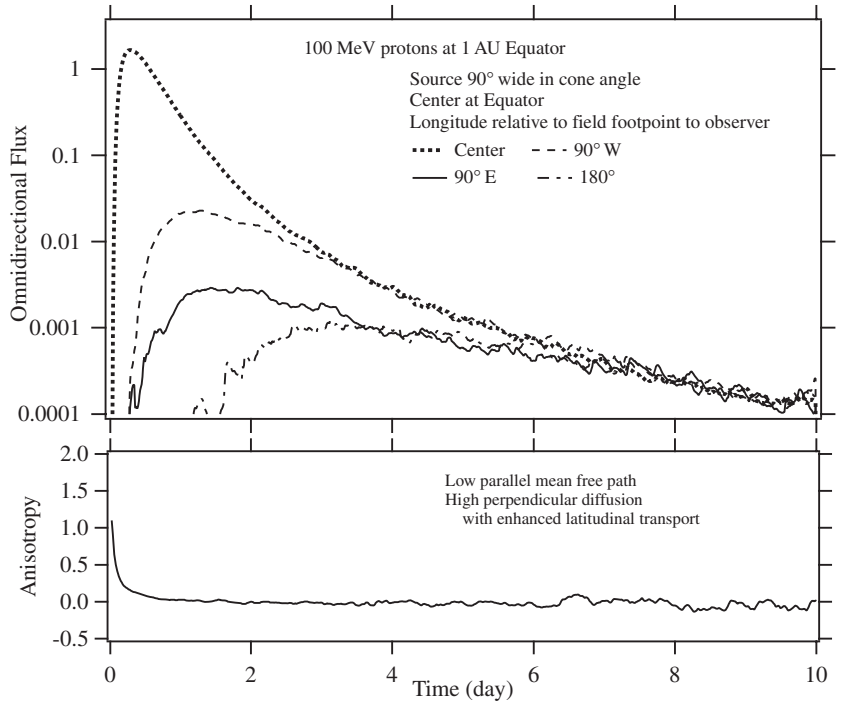

Figure 24. Omnidirectional flux and anisotropy at four different longitude locations at 1 AU Equator. A uniform source of 90° wide cone angle is centered at the Equator. The calculations use a low parallel mean free path and an enhanced latitudinal perpendicular diffusion.

rays modulation. We probably will not have much leverage in the outer heliosphere, because modulation of cosmic rays observed at Earth is sensitive to perpendicular diffusion in the region beyond the Earth's orbit. We probably can increase the latitudinal diffusion in the inner heliosphere. We have used a very low perpendicular to parallel diffusion ratio near the Sun. If we increase perpendicular diffusion there, it is very effective to drive particles diffuse across latitude because the distance in the latitudinal direction scales as r. An enhanced diffusion near the Sun will have similar effect from a uniform solar source on the Sun. Since such a measure will affect both longitudinal and latitudinal transport, constraints from longitudinal inhomogeneity of SEP flux should be considered at the same time.

Figures 24–28 show calculation results with enhanced latitudinal transport. The radial mean free path from the parallel transport is 0.05 AU. Perpendicular diffusion coefficient in the plane containing the Parker spiral magnetic field line has a $\kappa_0 = 5 \times 10^{20}$ cm^2 s^{-1}, while the perpendicular diffusion in the latitudinal direction is four times this value. In Figures 24 and 25, a uniform solar particle source covering a cone angle of 90° wide is centered at the Equator. The time profiles of SEP flux and anisotropy at various longitudes at 1 AU Equator are shown in Figure 24. Figure 25 shows the flux and anisotropy at various longitudes at 3 AU 60° high latitude. From Figures 24 and 25, we can see that the longitudinal uniform SEP flux is reached within a few days after the onset and the anisotropy remains the same independent of perpendicular diffusion and magnetic connection between the source and observer. Figures 26 and 27 show the flux and anisotropy calculations if the source particles of 90° wide cone angle is centered at high latitude 60°. The main features remain the same. Figure 28 compares the time

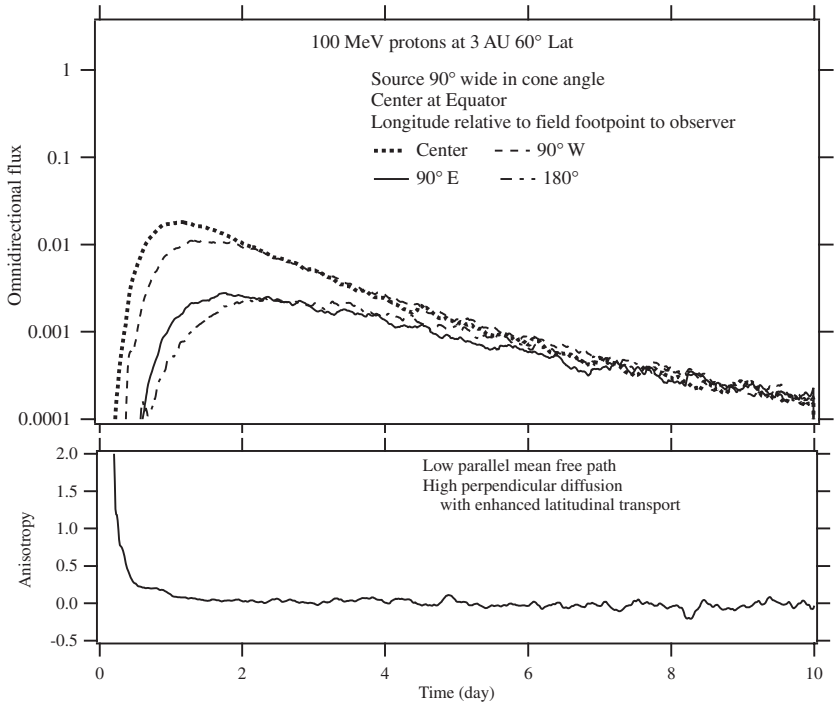

Figure 25. Same as Figure 24 except for four longitude locations at 3 AU 60° latitude.

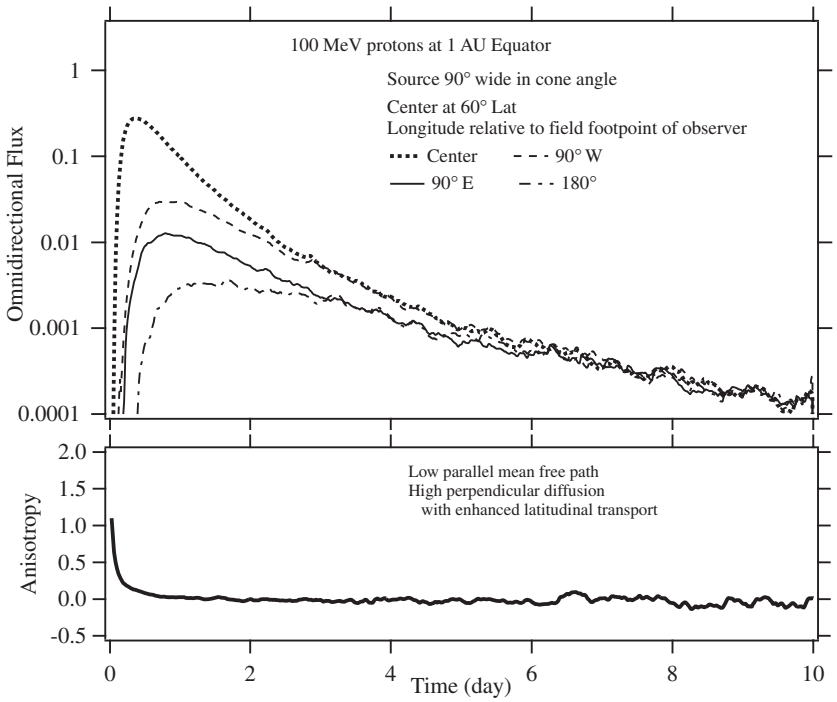

Figure 26. Same as Figure 24, with the solar particle source now centered at 60° latitude.

profiles of the SEP flux between 1 AU Equator and 3 AU 60° high latitude. A latitudinal uniform flux is reached in a few days if the solar source is centered at the Equator (top panel), but if the source is centered at high latitude 60°, the flux at 3 AU 60° is still ~ 2 higher than at 1 AU Equator in the decay phase. The reason is that latitudinal transport in terms of cosine of latitude in the given form of perpendicular diffusion coefficient at high latitudes is less efficient than at low latitudes (see Figure 22). Perhaps this difference is good enough to explain the observed reservoir phenomenon. Further latitudinal uniformity of SEP flux requires more increase of latitudinal transport at high latitudes. We leave this for future studies in connection with analysis of particular SEP events.

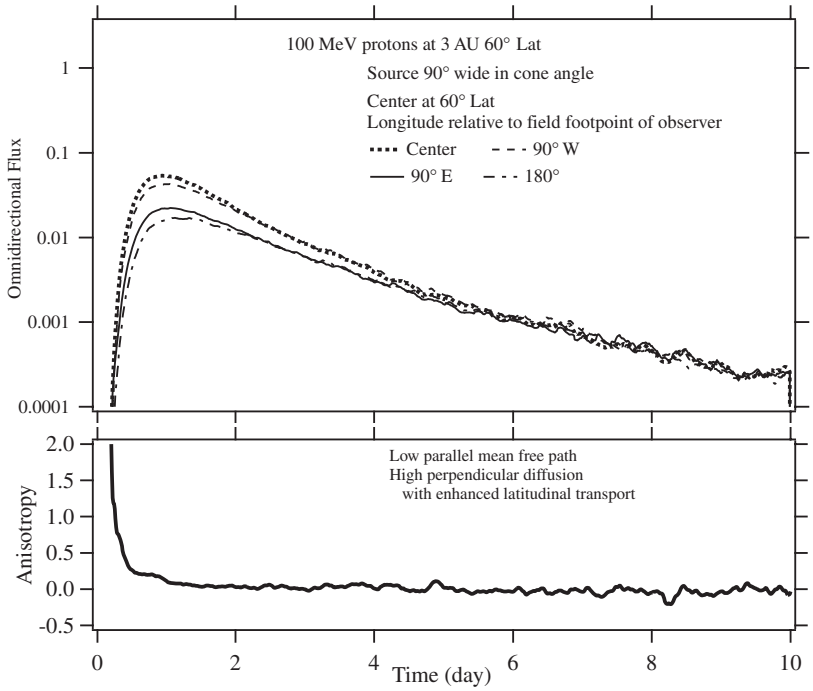

Figure 27. Same as Figure 26 except at 3 AU 60° latitude.

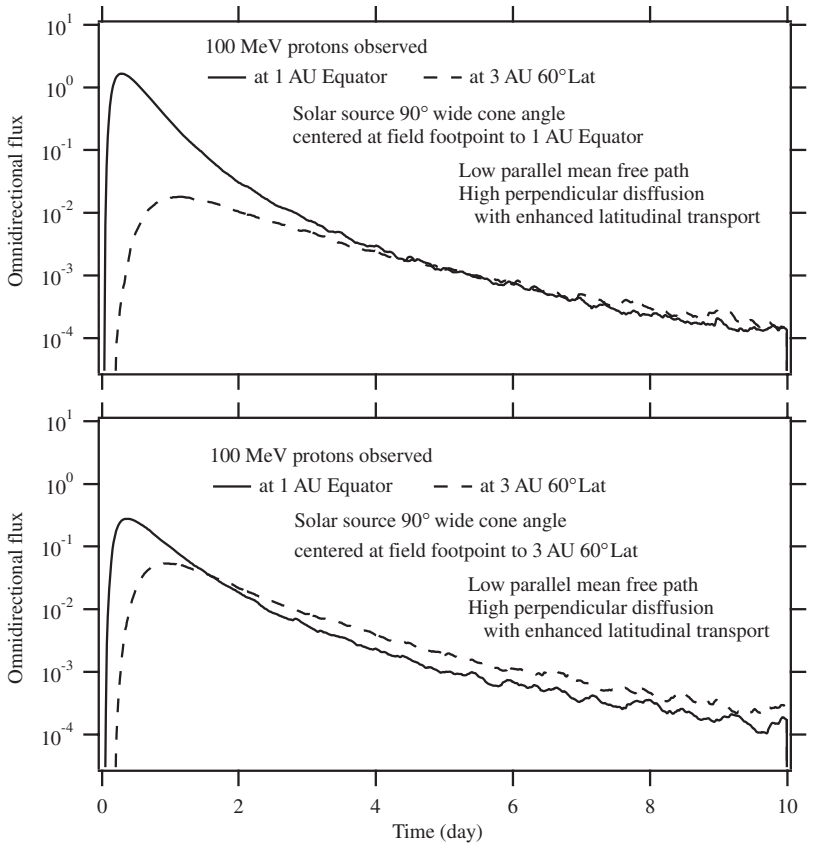

Figure 28. Comparison of omnidirectional fluxes at 1 AU Equator and 3 AU 60° latitude. The calculations use a low parallel mean free path and an enhanced latitudinal perpendicular diffusion.

4. SUMMARY

We have presented a model calculation of SEP propagation in a realistic three-dimensional interplanetary magnetic field. Our model includes essentially all the particle transport mechanisms. In this first model run, we find that the observed SEP reservoir phenomenon is a robust result of SEP propagation with an enhanced "communication" across latitude and longitude. The following are few major features of SEP interplanetary propagation in three dimension. These conclusions apply to SEPs that are produced near the Sun and released into interplanetary space all at once initially.

1. Adiabatic cooling plays an important role in SEP propagation in interplanetary space. Its effects can show up in SEP flux as early as half a day. It is the most dominant mechanism that controls the dissipation SEPs from the inner heliosphere. Most of adiabatic cooling occurs near the Sun.
2. Without perpendicular transport, the time profile of SEP flux observed at any location in the heliosphere is sensitive to the longitudinal distribution of the solar source at the latitude of the observer.
3. If the solar source injection is uniform on the Sun, it is possible that SEPs can reach a uniform reservoir in the inner heliosphere without particle perpendicular diffusion in interplanetary space. Larger parallel mean free path will make it easier to reach a uniform reservoir. This happens because dissipation of SEPs is dominated by adiabatic cooling which is most effective near the Sun where all the field lines are identical. Large parallel mean free paths ensure that the observed particles are easily assessable to the inner region of rapid adiabatic cooling. With sufficiently large mean free paths, all particles with different energies will dissipate roughly at the same rate. If this is the cause of uniform reservoir, it implies that the latitudinal and longitudinal transport of SEPs occurs in the corona before they are released into interplanetary space. However, any observation of longitudinal or latitudinal inhomogeneity of SEP fluxes at the beginning of an SEP event may invalidate this scenario.
4. Perpendicular diffusion, at the level inferred from observations of cosmic ray modulation at Earth, can greatly smooth out inhomogeneities of SEP fluxes from the solar source. With perpendicular diffusion, particles may appear many days before the magnetic field lines that connect to the solar source arrive and particles may even come from an event on the opposite side of direct magnetic connection site. It is easier to reach longitudinal uniformity at larger radial distance.
5. Perpendicular diffusion can smooth out longitudinal variation more easily than it does to latitudinal variation. With the given value of perpendicular diffusion inferred from cosmic ray modulation, SEP fluxes still show some latitudinal variation after 10 days. An enhanced latitudinal transport is required in order to reproduce a more uniform reservoir at all latitudes if the latitudinal transport occurs in interplanetary space.
6. Anisotropy of particle flux is not affected by perpendicular diffusion or direct magnetic connection to the solar source. Significant anisotropy only appears in an event that has direct magnetic connection near the time of event onset or initial particle injection but not at the onset of SEP fluxes. If an increase of SEP flux is brought in by convection of magnetic flux tubes that are filled with SEPs or by perpendicular diffusion, the event will not show significant anisotropy. Anisotropy can be a robust test of direct magnetic connection to a solar particle source and the level of parallel mean free path in interplanetary space.

We are grateful to M. Hohlmann and C. Fulton for providing their computer clusters used in this calculation. We thank Chinese National Science Foundation for partial support under grants NNSFC 40621003, 40674095 and 40523006. This work was supported in part by NASA under Grants NAG5-13514, NNG06G122G, NNX07AH16G, and JPL contract 1240373.

REFERENCES

Beeck, J., & Wibberenz, G. 1986, ApJ, 311, 437
Bieber, J. W., Matthaeus, W. H., Smith, C. W., Wanner, W., Kallenrode, M.-B., & Wibberenz, G. 1994, ApJ, 420, 294
Droge, W. 1994, ApJS, 90, 567
Dwyer, J. R., et al. 1997, ApJ, 490, L115
Giacalone, J., & Jokipii, J. R. 1999, ApJ, 520, 204
Hundhausen, A. J. 1993, J. Geophys. Res., 98, 13177
Isenberg, P. A. 1997, J. Geophys. Res., 102, 4719
Jokipii, J. R. 1966, ApJ, 146, 480
Kallenrode, M.-B. 1993, J. Geophys. Res., 98, 19037
Kallenrode, M.-B., & Wibberenz, G. 1997, J. Geophys. Res., 102, 22311
Kloeden, P. E., & Platen, E. 1992, Numerical Solution of Stochastic Differential Equations (Berlin: Springer)
Kota, J., & Jokipii, J. R. 1995, Science, 268, 1024
Lario, D., et al. 2003, Adv. Space Res., 32, 579
Lee, M. A. 1983, J. Geophys. Res., 88, 6109
Lee, M. A. 2005, ApJS, 158, 38
Li, G., Zank, G. P., & Rice, W. K. M. 2003, J. Geophys. Res., 108, SSH 10-1
Maclennan, C. G., Lanzerotti, L. J., & Gold, R. E. 2001, Space Sci. Rev., 97, 281
Matthaeus, W. H., Qin, G., Bieber, J. W., & Zank, G. P. 2003, ApJ, 590, L53
Mazur, J. E., Mason, G. M., & Stone, E. C. 2000, ApJ, 532, L79
McKibben, R. B. 1972, J. Geophys. Res., 77, 3957
McKibben, R. B., et al. 2003, Ann. Geophys., 21, 1217
Ng, C. K., & Reames, D. V. 1994, ApJ, 424, 1032
Ng, C. K., Reames, D. V., & Tylka, A. J. 1999, Geophys. Res. Lett., 26, 2145
Ng, C. K., Reames, D. V., & Tylka, A. J. 2003, ApJ, 591, 461
Parker, E. N. 1963, Interplanetary Dynamic Processes (New York: Interscience)
Potgieter, M. S., Haasbroek, L. J., Ferrando, P., & Heber, B. 1997, Adv. Space Res., 19, 917
Potgieter, M. S. 1998, Space Sci. Rev., 83, 147
Press, W. H., Teukolsky, S. A., Veterling, W. T., & Flannery, B. P. 1991, Numerical Recipes (Cambridge: Cambridge Univ. Press)
Qin, G. 2002, PhD thesis, Univ. Delaware
Qin, G. 2007, ApJ, 656, 217
Qin, G., Matthaeus, W. H., & Bieber, J. W. 2002, ApJ, 578, L117
Qin, G., Zhang, M., Dwyer, J. R., Rassoul, H. K., & Mason, G. M. 2005, ApJ, 627, 562
Qin, G., Zhang, M., Dwyer, J. R., & Rassoul, H. K. 2004, ApJ, 609, 1076
Qin, G., Zhang, M., & Dwyer, J. D. 2006, J. Geophys. Res., 111, A08101
Reames, D. V., Kahler, S. W., & Ng, C. K. 1997, ApJ, 491, 414
Reid, G. C. 1964, J. Geophys. Res., 69, 2659
Rice, W. K. M., Zank, G. P., & Li, G. 2003, J. Geophys. Res., 108, SSH 5-1
Roelof, E. C. 1969, in Lectures in High Energy Astrophysics, ed. H. Ogelmann & J. R. Wayland (Washington, DC: NASA), SP-199, 111
Roelof, E. C., Gold, R. E., Simnett, G. M., Tappin, S. J., Armstrong, T. P., & Lanzerotti, L. J. 1992, Geophys. Res. Lett., 19, 1243
Ruffolo, D. 1995, ApJ, 442, 861
Schlickeiser, R. 2002, Cosmic Ray Astrophysics (Berlin: Springer)
Shalchi, A., Bieber, J. W., Matthaeus, W. H., & Qin, G. 2004, ApJ, 616, 617
Skilling, J. 1971, ApJ, 170, 265
Zank, G. P., Rice, W. K. M., & Wu, C. C. 2000, J. Geophys. Res., 105, 25079
Zhang, M. 1999, ApJ, 513, 409
Zhang, M. 2005, ApJ, 624, 1038
Zhang, M. 2006, J. Geophys. Res., 111, A04208
Zhang, M., Jokipii, J. R., & McKibben, R. B. 2003, ApJ, 595, 493